C. Climent, F. J. Garcia-Vidal y J. Feist. “Cavity-modified chemistry: towards vacuum-field catalysis”. Effects of electric fields on structure and reactivity: new horizons in chemistry. Ed. S. Shaik y T. Stuyver. Reino Unido: Royal Society of Chemistry, 2021. 343-393

DOI: https://doi.org/10.1039/9781839163043-00343

Chapter X. Cavity-modified chemistry: towards vacuum-field catalysis

C. Climentᵃ*, F. J. Garcia-Vidalᵃ and J. Feistᵃ.

ᵃ Departamento de Física Teórica de la Materia Condensada and Condensed Matter Physics Center (IFIMAC), Universidad Autónoma de Madrid, E-28049 Madrid, Spain

*corresponding email address: claudia.climent@uam.es

ABSTRACT

In the preceding chapters, electric field effects on chemical reactivity have been extensively discussed, focusing on STM setups and enzyme catalysis among many others. Here we will focus on a rather different and only recently explored approach to manipulate chemical reactions with electric fields. With the use of resonant cavity modes hosted in Fabry-Pérot cavities for instance, as well as plasmonic modes, very recent investigations have shown modifications of chemical reactivity and dynamics, including thermal reactions and photochemistry, as well as manipulation of materials

properties and nonadiabatic processes. All these works have given birth to a new field termed polaritonic chemistry due to the fact that in the so-called strong-coupling regime, polaritons become the new eigenstates of the system. These are hybrid states of light and matter that inherit properties from both constituents, providing new means to modify chemical phenomena. The aim of this chapter is two-fold: on one side provide a general background on confined light modes and strong coupling for the non-specialised reader, and on the other, review the recent achievements of the field, paying special attention to modifications in ground-state reactivity. To this end, the chapter is organized as follows. After an introduction to settle basic concepts, we review the most relevant experimental and theoretical work in which modified chemical reactivity has been reported and conclude with the challenges faced by the field.

X.1 Introduction

X.1.1 Glossary of terms and overview

Herein we provide several textboxes intended to complement the contents of the following sections. Textbox 1 summarizes the terms mentioned throughout this chapter that may be unfamiliar to a chemist audience. The two ways to modify chemical reactivity with confined light modes that are discussed in this chapter are depicted in Textbox 2. A summary of the electric field strengths involved is provided in Textbox 3. Finally, experimental setups to investigate the topics covered in this chapter are summarized in Textbox 4.

Textbox 1: Summary of physics terminology used throughout the chapter

- **Fock states**, also known as number states, represent those quantum states with a well-defined number of particles (i.e. *quanta*). For instance, the Fock state $|n\rangle$ describes the state of a system with exactly n excitations of energy $\hbar\omega$ each. The vacuum state is represented by $|0\rangle$ since no excitation is present. In Figure X.1 (right), the Fock states of a quantum harmonic oscillator are shown from zero up to five excitations ($n = 0 \ldots 5$).
- A **Fabry-Pérot cavity** consists of two parallel facing mirrors where multiple reflections lead to standing waves (see Figure X.1). These are known as the cavity modes. Each of these modes can be formally described as a quantum harmonic oscillator representing the possible excitations of the system. The Fock state $|1\rangle$ represents a cavity mode with one excitation, i.e., one photon.
- The **Casimir effect** refers to the attractive force that two parallel uncharged conducting plates experience when they are close to each other. This was predicted by Casimir in 1948 and has been verified experimentally. The Casimir force is related to the vacuum fluctuations of the electromagnetic field and may be derived within a quantum electrodynamics framework. Alternatively, the Casimir force may be understood as the relativistic and retarded Van der Waals force between two metal plates. Such retardation effects are relevant when the separations between the interacting bodies are much larger than the characteristic absorption wavelength due to the finite speed of light at which the fields propagate. Nowadays, the Casimir force adopts a broader meaning and usually refers to the interaction between two macroscopic bodies.
- The **Casimir-Polder force** is also a dispersion force closely related to the Casimir effect for the case of polarizable atoms (or molecules). It refers to either atom-atom (molecule-molecule) interactions or those between an atom (molecule) and a macroscopic body (e.g. conducting plate). For the specific case of a neutral polarizable molecule close to a small metal nanoparticle, their Casimir-Polder interaction potential corresponds to their Van der Waals interaction comprising the Debye and London forces.
- **Plasmons** are the collective excitations of conduction electrons in metals. In this book chapter, we are interested in surface plasmons on metal surfaces rather than in the bulk. Metal nanoparticles hold **localised surface plasmons** and these can be visualized as an electron density oscillating back and forth as shown in Figure X.5a. In flat surfaces, these plasmons propagate along the metal surface and are known as **surface plasmon polaritons** (Figure X.5b).
- Apart from simple geometries such as metal surfaces and spherical nanoparticles, more complex structures supporting plasmonic modes are of interest in polaritonic chemistry. For instance, metallic nanoprisms, arrays of nanoparticles, metal surfaces with hole arrays, bowtie nanoantennas or nanoparticles facing a flat surface in the so-called nanoparticle-on-mirror configuration (Figure X.6). Since in several of these configurations there are metal surfaces facing one another, just like the mirrors in Fabry-Pérot cavities, and because quantized plasmonic modes can be formally described as the photons confined in mirror-based cavities, the term **plasmonic nanocavities** is widely used to name such metallic nanostructures.

- **Polaritons** are coupled light-matter states arising from the strong interaction between electromagnetic modes and material excitations. Within the context of this chapter, when a bright molecular excited state is in resonance with a confined electromagnetic mode (either plasmonic or mirror-based cavities), if they interact fast enough before both excitations decay, then the so-called **strong coupling** regime is achieved. In such scenario, the excitations are no longer exclusively light or matter-like, but combined to yield hybrid states known as polaritons. For one molecular state interacting with one cavity mode, two polaritons are formed, namely the lower and upper polaritons. One can distinguish between either **electronic** or **vibrational strong coupling** depending on whether the confined electromagnetic mode interacts with an electronic transition or a vibrational mode of the molecule.
- The **Rabi frequency** in the strong-coupling regime corresponds to the energetic splitting between the upper and lower polaritons and quantifies the light-matter interaction strength.
- The **Jaynes-Cummings** model is a popular model used in quantum optics to study strong coupling between one atom and a single cavity mode. The **Tavis-Cummings** model is an extension of the Jaynes-Cummings model to describe collective strong coupling between more than one atom and a single cavity mode. Traditionally, in these models the atom is described as a two-level system. Currently, further complexity is considered, for instance, by including vibrations when investigating strong coupling with molecules.
- **Polaritonic chemistry** is an emerging field aiming to manipulate chemical reactivity,

Textbox 2: Routes to modify chemistry with confined light modes

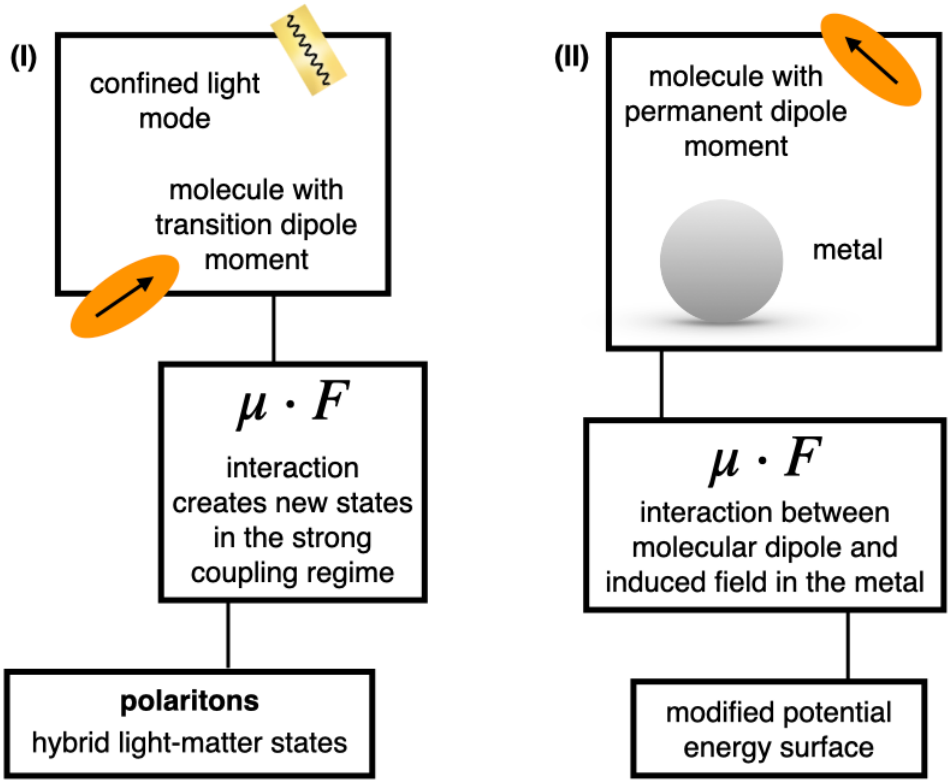

- In section X.2.1 we briefly discuss several examples where photochemistry has been manipulated under electronic strong coupling when a bright electronic molecular state was coupled to optical microcavity modes or plasmonic modes.
- In section X.2.2.1 we summarize recent experiments where the rate of thermal reactions has been modified by strongly coupling IR cavity modes to molecular vibrations under the so-called vibrational strong coupling regime.
- Both of these examples where photochemistry as well thermal reactions have been modified under electronic or vibrational strong coupling are a consequence of the formation of polaritons as shown in route (I). In this situation, the interaction between the electric field of the confined light mode and either electronic or vibrational transition dipole moments results in molecular states that become mixed with the light mode, leading to a novel way to manipulate ground and excited-state chemistry.
- The theory developed by our group to understand the experiments under vibrational strong coupling is discussed in section X.2.2.2. Our results suggest that chemical reactions can be catalysed by means of Casimir-Polder forces when molecules and metals interact, as show in route (II). In particular, for the simplified case of a molecule in close proximity to a plasmonic metallic nanosphere, its permanent molecular dipole moment will induce a dipole moment in the nanosphere. The interaction energy between the permanent dipole moment and the induced electric field in the metal will result in a modified potential energy surface that can be exploited to catalyse chemical reactions.

Textbox 3: Electric fields

- In quantum optics, the quantity that characterises the electric field strength of a cavity mode is the single-photon electric field $\boldsymbol{F_{1ph}}$ (equation X.2). For the light-matter coupling constants used throughout this chapter, the corresponding F_{1ph}~0.1-0.2 V/Å.
- It should be noted that these quantised field strengths $\boldsymbol{F_{1ph}}$ are not directly comparable with static fields, although they could be compared to classical oscillating fields, given that they are related to the electric field fluctuation of the vacuum state. The relevant energies are given by the dot product of the 1-photon field strength $\boldsymbol{F_{1ph}}$ with the molecular transition dipole $\boldsymbol{\mu}$, and correspond to the Rabi splitting $\hbar\Omega_R$ observed in the experiments.
- Regarding the induced electric fields of route (II) in Textbox 2, the cavity-induced energy-shift of the permanent molecular dipole is given by $-\frac{1}{2}\boldsymbol{F_{induced}}\cdot\boldsymbol{\mu}$. Since according to equation X.11, the Debye energy-shift term of the Casimir-Polder interaction is given by $-\frac{1}{2}(\boldsymbol{\lambda}\cdot\boldsymbol{\mu})^2$, then $F_{induced}=\lambda^2\mu$, where we have assumed that the permanent dipole moment and the cavity mode polarisation are aligned. Therefore, for coupling strengths λ of 0.02 a.u. and dipole moments of the order of 1 a.u., $F_{induced}$~0.02 V/Å.

Textbox 4: Experimental realisations

- To investigate how the rate of chemical reactions is modified under vibrational strong coupling, the common procedure is to use a microfluidic Fabry-Pérot cavity (Figure X.4b). It is important to realize that such cavities contain two mirrors and that the cavity mode resonances are dictated by their separation. Therefore, the cavity should be probed to verify that the system is under vibrational strong coupling. In a microfluidic setup, the reaction mixture flows through the cavity and two common routes are often used to monitor the course of the reaction: (i) record the shift of a higher-order cavity mode and relate it to the product concentration if the refraction index changes during the reaction, and (ii) monitor an electronic absorption band of either a reactant or product.
- To experimentally achieve the catalysis of chemical reactions with Casimir-Polder interactions in plasmonic nanocavities, the reactants could be placed in solution with the metallic nanostructures. The challenge here would be to isolate Casimir-Polder effects from chemisorption on the metal surface that may also contribute to catalysis. In addition, strategies to control the position of the molecules relative to the electric field of the plasmonic modes should be pursued to maximize catalytic effects.
- It is important to stress that in both approaches, either with vibrational strong coupling or Casimir-Polder interactions, the system does not need to be excited with a laser.

X.1.2 Confined light modes

Let us begin by addressing the following question: What are confined light modes? These refer to electromagnetic modes which are confined in space, and due to this property, their interaction with matter can be significantly enhanced. This can happen for instance in optical resonant cavities such as Fabry-Pérot microcavities (Figure X.1) where two mirrors are placed very close to each other with a separation of the order of micrometers.[1] Light trapped inside this cavity will experience multiple reflections and, for those frequencies where constructive interference dominates, standing waves will arise. These electromagnetic waves are just like the solutions of a particle in a box, that is, a rope with fixed ends describing a sine function with multiple nodes (Figure X.1). More precisely, each of these solutions with increasing number of nodes are the cavity modes and their excitations correspond to confined photons.

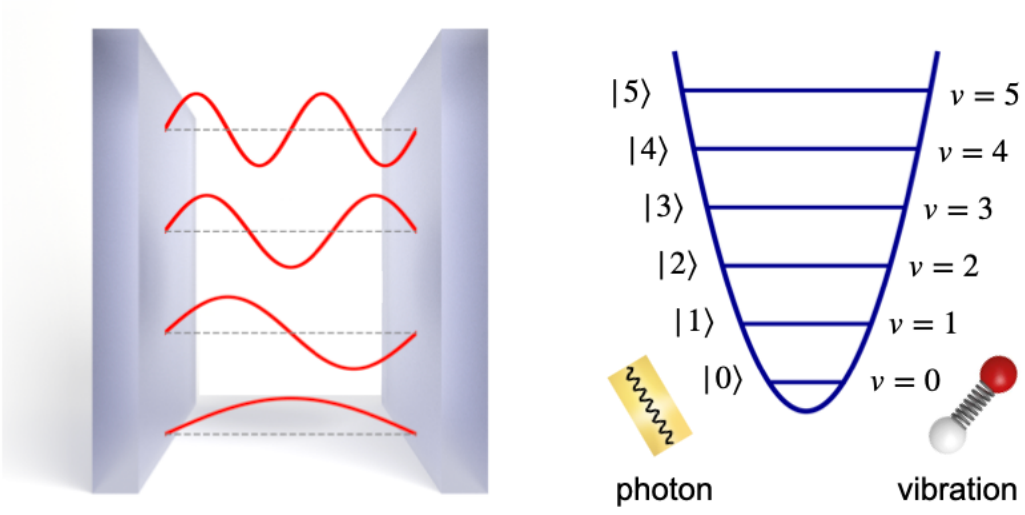

Figure X.1 Sketch of a planar cavity formed by two facing mirrors showing several cavity modes with increasing number of nodes. An analogy between the Fock states of a cavity mode is made with the levels of a vibrational mode of a molecule.

An alternative way to think about cavity modes is by making an analogy with molecules. Just like molecules have several vibrational modes and each of these modes is described by a series of states (ground vibrational level and a ladder of vibrationally excited states), a resonant cavity has a series of cavity modes, each of them consisting of a ladder of states (Figure X.1). The ground state of a cavity mode is called the vacuum state, and represents the situation with zero photons, i.e., $|0\rangle$, while the excited states up the ladder correspond to a cavity mode with increasing number of photons, $|1\rangle$, $|2\rangle$, … As we will see later on, this analogy with vibrational modes is very suitable given that confined light modes can be formally described as harmonic oscillators.[2]

A very interesting and important aspect of cavities is that, even when they are "empty", meaning that there are no photons in the cavity, the cavity modes exist. In other words, the modes are intrinsic to the cavity without the need for light to be explicitly trapped inside, in the same way that the excited states of a molecule exist even if they are not populated. If the light-matter interaction, i.e., the interaction between the cavity states and the molecular states, is large enough, the matter energy levels are affected even "in the dark". This is a very appealing feature that, as we will see, allows to manipulate chemical phenomena with cavities without the need to explicitly excite the system with an external light source. In order to get an intuitive understanding of this effect and provide a general context for the reader, in the following we will qualitatively discuss an important result from the field of quantum electrodynamics.

Similarly to quantum physics where we learn that matter (atoms, molecules…) has discrete energy levels, in the field of quantum electrodynamics[2] the electromagnetic (EM) field is quantized, and therefore, provides a framework for a

quantum description of light-matter interactions. Quantum electrodynamics tells us that the EM field is composed of modes, and that photons are the excitations of these modes. Therefore, our previous qualitative description of the ladder of states of a cavity mode is in fact general to any EM mode. Another important result from quantum electrodynamics is that, as commented above, EM modes can be described as harmonic oscillators, just like molecular vibrations. A very important consequence of this fact is that there is a zero-point energy associated with the vacuum state of the EM field. Even more interestingly, when one works out the expectation values of the field operators (i.e. $\hat{F}$=electric and magnetic), it turns out that in the vacuum state, the expectation value of the field is zero, $\langle \hat{F} \rangle = 0$, meaning that the mean of the outcome of several measurements would be that there is no field in the vacuum state. However, the expectation value of the square of the field operator does not vanish, $\langle \hat{F}^2 \rangle \neq 0$, and therefore, there is an uncertainty ΔF associated to the vacuum state of the EM field since these quantities are related by $\left(\Delta \hat{F}\right)^2 = \langle \hat{F}^2 \rangle - \left\langle \hat{F} \right\rangle^2$. Although apparently there is no EM field in the vacuum state, in fact the EM field is constantly fluctuating, and these vacuum field fluctuations have measurable effects.[3] Just to give some examples of their relevance, vacuum fluctuations are responsible for the Lamb shift observed in the microwave spectrum between two atomic hydrogen levels.[4] They also lie at the core of the Casimir effect,[5] where metal or dielectric plates experience physical forces arising from such fluctuations. Another example more closely related to chemistry is that of Van der Waals interactions which are also due to vacuum fluctuations.[6]

The previous discussion on the EM vacuum state also applies to optical resonant cavities, and in particular, the electric field fluctuation for a single-mode cavity in the state $|n\rangle$, i.e., with n photons present, is given by[7]

$$\Delta\langle\hat{F}\rangle = \sqrt{\frac{\hbar\omega_c}{2\epsilon_0 V}}\sqrt{2n+1} \quad \text{(X.1)}$$

where $\hbar\omega_c$ is the cavity mode energy, ϵ_0 is the vacuum permittivity, V is the (effective) mode volume which refers to the space in which the field is concentrated, and n is the number of photons in the cavity. For an "empty" cavity, i.e. the vacuum state with $n = 0$ where no photons are present, fluctuations do not vanish.

Up to now, we have discussed confined light modes in general, and presented Fabry-Pérot cavities as an example. However, there are many different platforms that can be used to confine EM modes, with widely varying properties, in particular regarding the strength of the confinement (reflected in the mode volume V) and the lifetime of the photons in the cavity (normally expressed through the quality factor Q, the ratio between the dissipation rate, κ, and the frequency, ω). In particular, plasmonic modes in metal nanostructures provide the strongest field confinements (smallest mode volumes) achieved up to now.[8] Plasmons can be thought of as the excited states of metals involving collective oscillations of the conduction electrons, and confine EM excitations on extremely small scales at metal-dielectric interfaces. Nowadays, refined fabrication techniques allow the design of a wide variety of complex metallic structures at the nanoscale capable of localising EM modes in very deep subwavelength volumes (with mode volumes six or more orders of magnitude smaller than in typical mirror-based microcavities), such that the per-photon fields are strongly enhanced.[9] Many types of plasmonic structures are commonly used, for instance, metallic nanoparticles supporting localized surface plasmon resonances (Figure X.2a). The propagating counterpart of these localized resonances can be found at the extended interface between a metal and a dielectric material (Figure X.2b), the so-called surface plasmon polaritons.[10,11] Plasmonic modes can be seen as strongly confined EM field modes,

and for our purposes can then be thought of and treated just like cavity modes.[12] Consequently, such structures are nowadays often called plasmonic "nano-cavities" even if the light confinement is not due to a conventional cavity structure with mirrors. Before discussing several concrete examples of such structures, we first give an introduction on strong coupling between molecules and confined light modes.

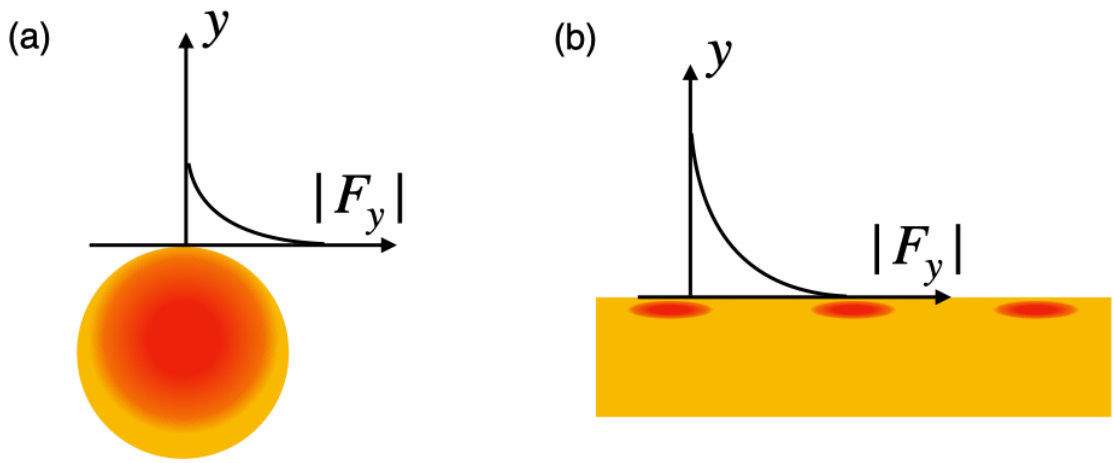

Figure X.2 Sketch of a (a) localized surface plasmon of a spherical nanoparticle and (b) surface plasmon polariton at a metal-dielectric interface. The electric field profile along the surfaces is also schematically shown. Adapted from Ref. 13 under the terms of the Creative Commons Attribution License CC BY 4.0 (https://creativecommons.org/licenses/by/4.0/legalcode), Copyright 2012.

X.1.3 Introduction to strong coupling

Let's imagine we place a molecule with a bright singlet excited state inside a Fabry-Pérot cavity. By tuning the separation between the mirrors one can make a cavity mode resonant with the molecule's excited state. It is important to highlight that physically, single-molecule strong coupling at room temperature cannot be achieved with planar cavities because the light-matter coupling strength is too weak,[8] but

nonetheless, it serves for illustrative purposes. In this situation, if the interaction between the cavity mode and the molecular transition is strong enough compared to the losses of the system, strong coupling between them may be achieved, leading to the formation of two hybrid light-matter states known as polaritons (Figure X.3a). These states are mixtures of both the cavity mode and the molecular excitation, and in the absorption spectrum of the coupled system, the original absorption band of the molecule or the cavity mode splits into two peaks due to the lower and upper polaritons (LP & UP). The energetic separation between these two states is known as the Rabi splitting $\hbar\Omega_R$, and quantifies the strength of the light-matter interaction.

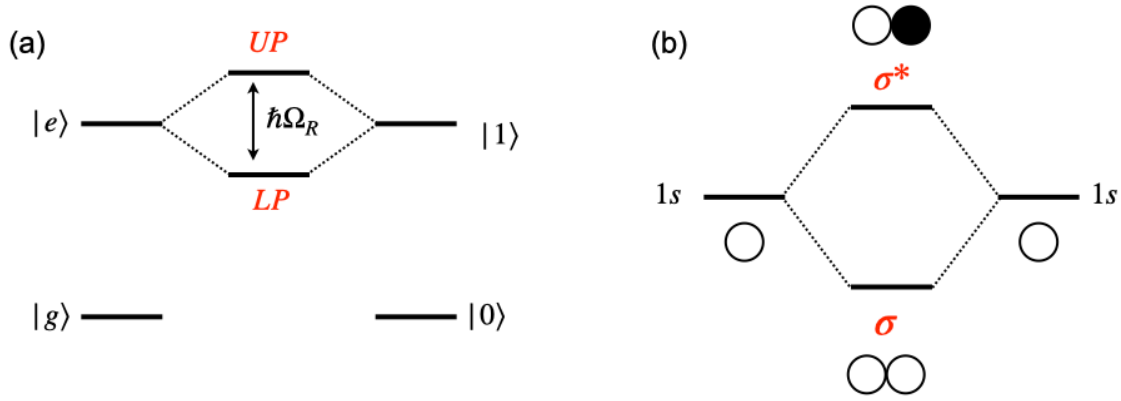

Figure X.3 (a) Diagram showing the formation of the lower and upper polaritons (LP & UP) under strong coupling between an excited state of a molecule and a cavity mode. The Rabi splitting ($\hbar\Omega_R$) between the polaritons is also shown. Legend: $|g\rangle$ and $|e\rangle$ represent the ground and excited state of the molecule, while $|0\rangle$ and $|1\rangle$ represent the cavity mode with no-photons and one photon. (b) Molecular orbital diagram showing the formation of the σ and σ* orbitals from the combination of two 1s atomic orbitals of two hydrogen atoms.

Such hybridisation between cavity modes and molecular states can be understood very intuitively by thinking in terms of atomic orbitals and how they combine into molecular orbitals in molecules. For instance, in the hydrogen molecule, the two degenerate 1s orbitals mix in an in-phase and out-of-phase fashion leading to the σ and σ^* molecular orbitals (Figure X.3b). In the cavity situation, the bare cavity and molecular modes would play the role of the atomic orbitals while the mixed polariton states would play that of the molecular orbitals. However, in the hybrid cavity-molecule system, there is a very rich additional phenomenology due to the hybrid nature of the polaritons, which inherit properties from both their light and their matter constituents, leading to a variety of unexpected phenomena.[14]

Another way to visualize the formation of polaritons is the following. When the molecule in its ground state is placed inside the cavity together with one photon in a resonant cavity mode, the molecule will absorb the photon, then emit it, absorb it again, and so on. Since the initial state (ground-state molecule + photon in the cavity) is not stationary but undergoes oscillatory dynamics, this implies that it is not an eigenstate of the system. The actual eigenstates of the system cannot be assigned to the different subsystems (molecule or cavity), but are mixtures of excitations in both systems. Within this picture, if one tracks the excited state population of the molecule, so-called Rabi oscillations will appear, reflecting the fact that the photon is repeatedly absorbed and emitted. The frequency of these oscillations is given by the Rabi frequency Ω_R, which in the energy domain is exactly the Rabi splitting between the polariton energies.

For the system to be in strong coupling and form polaritons we previously stated that the interaction between the cavity mode and the molecular excited state should be strong enough. But how strong is strong enough? Just like molecular excited states have a finite lifetime due to radiative and non-radiative relaxation processes, cavity

modes also have a finite lifetime due to leakage outside the cavity and other manufacturing imperfections. Consequently, the strong-coupling regime is reached when their interaction, i.e., Rabi frequency, is faster than the respective lifetimes of the cavity mode and the molecular excited state, and so they both have enough time to interact before they decay. A common criterion adopted to certify that the system is under strong coupling is to compare the Rabi splitting with the linewidth of the molecular absorption band or that of the cavity modes. If the Rabi splitting exceeds the linewidth, then this means that the interaction is faster than the decay processes and so the strong coupling regime is reached. However, one must be cautious with molecules, since in this case the linewidth is not only determined by the natural lifetime, but arises due to a combination of factors such as inhomogeneous broadening and, in particular, molecular vibrations and rotations. If the interaction between light and matter is not strong enough, then the system is said to be in the weak-coupling regime. In this situation, hybrid states are not formed but interesting things also occur. In particular, the radiative decay rate of the molecule can be altered since it feels a modified electromagnetic environment inside an optical cavity compared to outside. This modification is known as the Purcell effect.[15] While it will not be treated in detail here, we mention that when the Rabi frequency is comparable with the transition frequency of the system, the system is said to be in the so-called ultrastrong coupling regime.[16] As a side note, “ultrastrong” and “strong” coupling are determined by different criteria, and it is possible for a system to be in ultrastrong coupling but not in strong coupling.

So far we have described the interaction of a cavity mode with a molecular excited state. This is known as electronic strong coupling, and as we will discuss in the second part of this chapter, there are several experiments reporting modified

photochemistry in such scenarios with both optical cavities as well as plasmonic modes. In addition, instead of coupling to electronic states of molecules, one can also couple to vibrational modes within vibrational strong coupling (VSC).[17] This offers many possibilities in terms of modifying ground state chemical reactivity, and as we will discuss, several works have demonstrated catalysis and inhibition of thermal reactions within VSC. It is important to point out that in electronic strong coupling, excitation energies (on the order of a few eV) are much higher than thermal energies (~26 meV at room temperature), and the excited states must be populated by some external source such as a laser in order to initiate a reaction or photophysical process. In contrast, in VSC, the involved energies are much lower (at most a few hundred meV) and experiments on chemical reactivity can be performed without applying any external driving to the system.

Under strong coupling, the general expression for the Rabi frequency when the light-matter interaction is treated within the dipole approximation is given by $\Omega_R = 2\hat{\boldsymbol{\mu}} \cdot \boldsymbol{F_{1ph}}$, where $\hat{\boldsymbol{\mu}}$ is the dipole moment operator and the single-photon electric field strength $\boldsymbol{F_{1ph}}$ reads[7,18]

$$\boldsymbol{F_{1ph}} = \sqrt{\frac{\hbar\omega_c}{2\epsilon_0 V}}\,\boldsymbol{e_F} \tag{X.2}$$

This is nothing else but the previously discussed electric field fluctuation for the vacuum state of a single-mode cavity with polarization unit vector $\boldsymbol{e_F}$. It is important to realise that $\boldsymbol{F_{1ph}}$ is related to the *effective* mode volume V that is somehow a measure of the volume within which the photon is confined, and thus depends on the cavity geometry. According to this expression, the light-matter interaction is therefore due to the interaction between the vacuum field and the transition dipole moment between

either electronic or vibrational states, depending on whether the system is under electronic or vibrational strong coupling. Moreover, the coupling strength will be maximized if the transition dipole moment is aligned with the polarization of the cavity mode. The fact that typical values of electronic transition dipole moments differ from vibrational ones reflects the different energy scale of electronic and vibrational strong coupling. In electronic strong coupling the Rabi frequency is given by $\Omega_R = 2\boldsymbol{\mu_{ge}} \cdot \boldsymbol{F_{1ph}}$, where $\boldsymbol{\mu_{ge}}$ is the transition dipole moment from the ground to the electronic excited state of the molecule. According to this expression, to reach electronic strong coupling, the molecular excited state must have a significant transition dipole moment. In VSC, after applying common approximations such as the Born-Oppenheimer and the harmonic approximation (i.e., potential quadratic in R) and that the permanent dipole moment is linear in R, the Rabi frequency (for low coupling) can be expressed as $\Omega_R = \boldsymbol{\lambda} \cdot \boldsymbol{\mu_g'}(R_0)$.[19] For convenience the light-matter coupling strength is defined by

$$\boldsymbol{\lambda} = \sqrt{\frac{2}{\hbar\omega_c}}\boldsymbol{F_{1ph}} \tag{X.3}$$

and $\boldsymbol{\mu_g'}(R_0)$ is the derivative of the ground state dipole moment in mass-weighted coordinates (i.e. $R \rightarrow R\sqrt{M}$) evaluated at the ground state minimum configuration R_0. Here we see that in order to couple a molecular vibration to a cavity mode, this vibration should be IR active.

One of the most striking features of strong coupling is that it is a collective effect. Up to now we have discussed strong coupling of a single molecule with a cavity mode. However, in reality, strong coupling with a single molecule can only be reached in deeply sub-wavelength plasmonic cavities with mode volumes on the order of 100 nm^3 (around $10^{-6}\lambda^3$). For an ensemble of N molecules under electronic or vibrational strong

coupling, the interaction strength is given by the collective Rabi frequency $\Omega_{R,N} = \sqrt{N}\Omega_R$ where Ω_R is the single-molecule Rabi frequency. This means that the larger the number of molecules under strong coupling, the stronger the light-matter interaction will be. Moreover, under collective strong coupling, the polaritonic states are delocalised amongst all the molecules coupled to the confined light mode, with such delocalisation being a direct consequence of the light-like nature of polaritons. Furthermore, given that $\Omega_{R,N} \sim \sqrt{N/V}$ where the $\sqrt{N}$ contribution comes from the collective nature while $\sqrt{1/V}$ comes from the single-photon electric field amplitude, for systems where the molecules fill the available space, $\Omega_{R,N}$ simply scales with the square root of the concentration of the sample and is independent of the mode volume itself. Therefore, under strong coupling experiments, one must aim to place as many molecules as possible in the volume where the EM field is confined. One of the advantages of using organic molecules for strong coupling is the high density they can achieve as compared to other materials as well as the large transition dipole moments they possess, ideal to enhance the collective Rabi frequency $\Omega_{R,N}$. Let us mention that although the majority of experiments are performed for a macroscopic ensemble of molecules where the light-matter coupling strength is enhanced, there is an interest in the community to pursue single-molecule strong coupling and, indeed, such experiments have been reported with plasmonic nanocavities.[20]

The first experiments where polariton splitting was actually observed were done with surface plasmons and reported in the 1980s.[21,22] However, these experiments were not framed within a strong-coupling context and therefore were not the ones driving the field forward. For many decades, the fields of quantum optics and cavity quantum electrodynamics studied strong coupling of atoms in cavities,[7] leading to the

Nobel prize of Prof. Haroche for his contributions on this matter. Solid-state physicists also became interested in strong coupling and new materials such as inorganic semiconductors and quantum dots were investigated in cavities.[23–26] In the late 1990s - early 2000s, electronic strong coupling with organic materials was pursued,[27,28] mostly with organic semiconductors, with several works focusing on the excited state dynamics and the role played by the so-called exciton reservoir,[29] which we will come back to shortly. But it has not been until the last decade that strong coupling with molecules has raised interest in the community with the purpose to modify chemical reactivity and nonadiabatic phenomena.[30–33]

X.1.4 Cavities and plasmons

Having discussed the basics of strong coupling, let us return to our previous discussion on cavities and plasmons and give a brief overview on the typical platforms used in strong coupling experiments. Let's start with planar cavities, and more specifically, Fabry-Pérot ones. These consist of two facing mirrors whose separation can be adjusted so that multiple reflections with constructive interference lead to standing waves that are the cavity modes. The wavelength of these modes is given by $\lambda = 2nL/m$, where n is the refractive index of the medium, L is the distance between the mirrors and m is a non-vanishing integer which identifies the order of the cavity mode, with $m-1$ nodes. The mirrors of these cavities are usually made of Ag, Au, or sometimes Al, and a wide range of frequencies can be covered, including IR, UV and Visible radiation.[1] The main limiting factor of the performance of Fabry-Pérot cavities in strong coupling experiments is the mirrors reflectivity, which limits the lifetime of the cavity modes. Therefore, when interested in electronic strong coupling with molecules,

this is a relevant issue given that molecular excited states have longer lifetimes compared to those of the cavity modes.

A very important point about cavity modes is that they have in-plane dispersion, meaning that their energy depends on the wavevector along the plane parallel to the mirrors, $k_{\parallel}$ (Figure X.4a). This is because the condition for constructive interference along the axis perpendicular to the mirrors fixes the out-of-plane wavevector $k_{\perp} = m\pi/L$. The dispersion relation of a wave propagating in a dielectric medium is given by $E(k) = \frac{\hbar c}{n}k$, where c is the speed of light. Therefore, the dispersion relation for the modes of a Fabry-Pérot cavity is given by

$$E(k_{\parallel}) = \frac{\hbar c}{n}\sqrt{k_{\parallel}^2 + \left(\frac{m\pi}{L}\right)^2} \tag{X.4}$$

which is parabolic for low $k_{\parallel}$. Moreover, since for an angle of incidence θ the in-plane wavevector is given by $k_{\parallel} = k\ sin\theta$, resonance can be achieved with a wide range of frequencies given by the dispersion relation depending on how the system is probed. Unlike cavity modes, molecular excitations are non-dispersive, i.e. they have a flat profile for all $k_{\parallel}$. When polaritons are formed in the strong coupling regime, if the molecular excitation is chosen to be resonant with $E(k_{\parallel}) = 0$, then the LP mostly inherits the non-dispersive nature of the molecular excitation while the UP is highly dispersive (Figure X.4a). A consequence of this dispersive nature is that the composition of both polaritons will only be symmetrical at $k_{\parallel} = 0$.

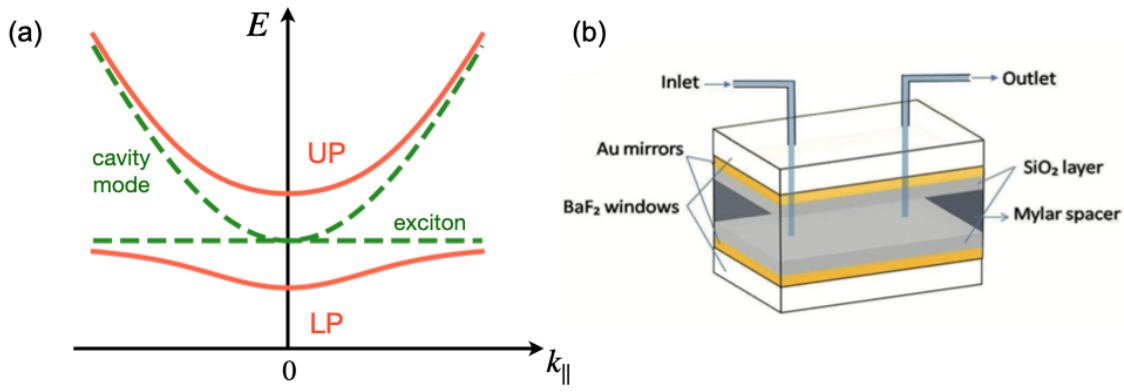

Figure X.4 (a) Polariton dispersion resulting from strong coupling between a cavity mode and a molecular transition. Note that both excitations are resonant at $k_{\|} = 0$. (b) Scheme of a microfluidic cavity used in vibrational strong coupling experiments. Reproduced from Ref. 34 with permission from Wiley-VCH, Copyright 2019.

In this chapter we will discuss several experiments investigating thermal reactions under vibrational strong coupling, therefore, it is of interest to briefly discuss the experimental setup. Typically, microfluidic Fabry-Pérot cavities such as that shown in Figure X.4b are used given that the reaction takes place in liquid phase, with an inlet and outlet allowing the reaction mixture to flow through the cavity. In this case, the separation between the two cavity Au mirrors can be adjusted by the use of a Mylar spacer. It is very common also to have an inert layer, e.g. SiO_2, deposited on top of the mirrors to prevent direct contact of the reactant solution with the metal surface. Finally, the whole cavity is encapsulated between two BaF_2 windows, suitable for probing purposes since they provide high transmission. In VSC experiments with these kinds of cavities, the common approach to monitor the reaction is to record the transmission spectrum. By taking advantage of the change in the refraction index of the medium as the reaction proceeds, the shift of the cavity modes frequency can be related to the appearance of the product.

Apart from Fabry-Pérot cavities, plasmonic nanocavities are also often used in strong coupling experiments, offering advantages as well as disadvantages with respect to optical cavities. Let us recall that *plasmonic nanocavities* refers to metallic structures supporting plasmonic modes. Since the physics describing coupling of an emitter to such modes is the same as that for standard mirror-based cavities, the term nanocavities is widely spread in the community. Regarding the advantages of plasmonic nanocavities vs Fabry-Pérot ones, the EM fields are much more confined in plasmonic nanostructures, leading to stronger light-matter interactions. However, plasmonic modes are very short-lived, given that electrons have many loss mechanisms. Basically, plasmonic modes decay within a few tens of femtoseconds or less.[8] This poses a serious drawback if one wishes to explore electronic strong coupling with molecules, since most photophysical and photochemical processes occur on longer timescales. For instance, molecular relaxation through conical intersections is a very fast and efficient process, and the ability to manipulate them with strong coupling is of prime interest in the field.[35–39] However, it is highly likely that the hybrid system will have already decayed through the metal losses before reaching the conical intersection. Nevertheless, given the stronger EM fields of plasmonic nanocavities compared to optical cavities, they are the ideal candidates to explore few or single-molecule strong coupling.[20] A typical quantity to characterise the field confinement is that of the mode volume already introduced previously. Although it is not always straightforward to calculate for plasmonic systems,[40] it still stands as a figure-of-merit. Typical mode volumes for standard cavities would be ~0.1 μm^3 , while for plasmonic ones they can be as small as 100 nm^3 or less.[9] Plasmonic nanocavities thus represent the only viable option for reaching single- or few-molecule strong coupling. The losses of the system are usually accounted for in what is known as the

quality factor Q, and both effects, the field enhancement and the losses are appraised in the so-called Purcell factor. [41]

Let us recall that surface plasmons can be excited at the interface between a metal and a dielectric, e.g., air. They are solutions of Maxwell's equations by imposing the appropriate boundary conditions for the geometry of interest. For highly symmetric systems, analytical solutions can be found, while for more complex structures, a typical approach is to resort to the transformation optics technique or numerical calculations.[42–44] In Figure X.5a, we give an example of a localised surface plasmon of a spherical metallic nanoparticle. Here we are showing the dipole plasmonic mode of the nanoparticle. However, just like molecules have more than one electronic excited state, this nanoparticle will also have a quadrupole mode and even higher order multipole modes, where the order of the mode is reflected by how the charge distributes on the surface due to the oscillation of the conduction electrons. Apart from localised plasmonic modes, plasmons that propagate along a metal surface also exist. For instance, propagating surface plasmons at the interface between a dielectric and a flat metal surface are known as surface plasmon polaritons. As shown in Figure X.5b, in this case, the enhanced fields also lie very near the metal surface but they propagate along it, in contrast to the modes of a localised nanoparticle. Typical materials used in these systems are noble metals such as Ag, Au, although Al and Cu are also used, with their plasmonic resonances lying in the infrared - visible range. In order to explore photochemistry under strong coupling, it still remains a challenge to have plasmonic resonances in the UV range. Regarding the dispersion relation of localized surface plasmons and surface plasmon polaritons, we refer the interested reader to reference 10.

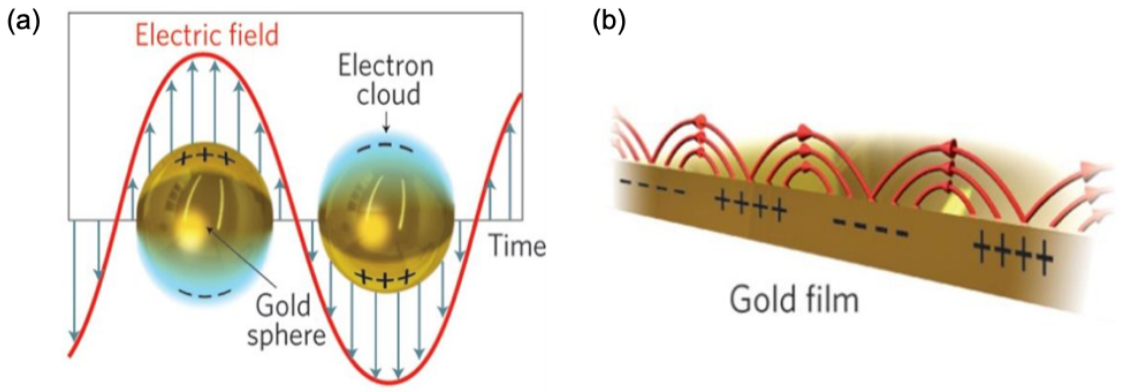

Figure X.5 (a) Localized surface plasmon in a gold nanoparticle. (b) Surface plasmon polariton at a flat gold–air interface. The dipolar mode of the spherical nanoparticle is shown and the field oscillations are also illustrated. Reprinted by permission from Nature, Ref. 45, Copyright 2011.

A metal nanoparticle and a metal surface are the simplest systems supporting surface plasmons, however, refined fabrication techniques have lately allowed the design of complex metallic nanostructures with extremely enhanced fields. For instance, few and single-molecule strong coupling has been recently achieved with a nanoparticle-on-mirror nanocavity.[20] In this system, a spherical gold nanoparticle with a 40 nm diameter was placed 0.9 nm above a 70 nm thick gold film (Figure X.6a). The authors were able to place a dye at the nanogap by encapsulating it within a cucurbit[n]uril macrocycle. Another very interesting system is the bowtie nanoantenna shown in Figure X.6b, where the face-to-face arrangement of both tips intensifies the fields at the gap. Plasmonic hole arrays or arrays of plasmonic nanoparticles (Figure X.6c and d) have also been used in strong coupling experiments.[46,47] These consist of metallic lattices of regularly spaced nanoparticles or holes and are very convenient to explore the effect of strong coupling in chemical processes since they are open cavities, meaning that a solution can be directly placed on the surface, or a layer of an

active material can be easily deposited. Moreover, their plasmonic resonances are easily tunable by varying the nanoparticle or hole size and their spacing in the lattice.

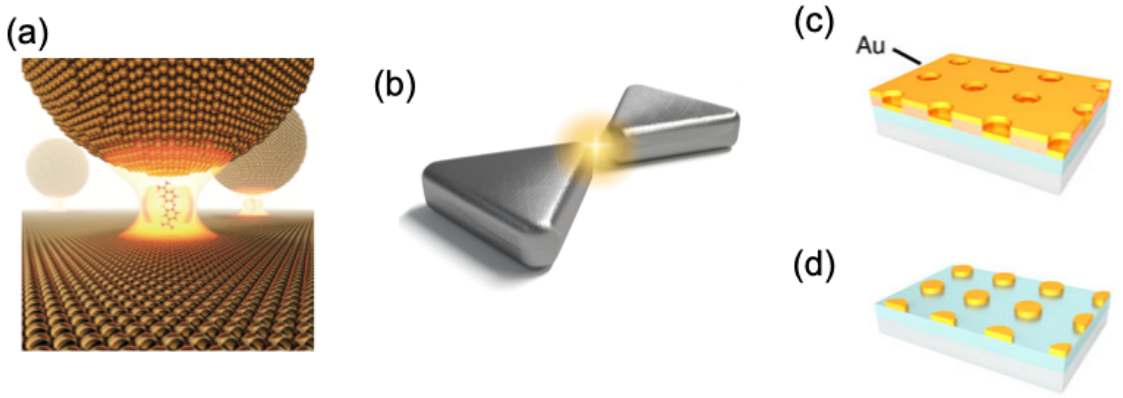

Figure X.6 Representative examples of plasmonic nanocavities such as (a) nanoparticle-on-mirror, (b) bowtie nanoantenna, and plasmonic (c) hole and (d) nanoparticle arrays. (a) Reprinted by permission from Nature, Ref. 20, Copyright 2016, (c) and (d) Reproduced from Ref. 48 under the terms of the Creative Commons Attribution License CC BY 4.0 (https://creativecommons.org/licenses/by/4.0/legalcode), Copyright 2015.

X.1.5 Models for strong coupling

Now that we have already introduced basic concepts on strong coupling, cavities and plasmons, let us conclude this section focusing on a simple model of strong coupling to illustrate the concepts introduced previously in a more quantitative manner. For our purposes, we will use a simplified description for the molecule and treat it as a two-level system. The standard model in quantum optics capturing the essential features of strong coupling is the Jaynes-Cummings model.[49] This model describes a two-level system interacting with a single cavity mode in the so-called rotating wave approximation.[2] The Jaynes-Cummings Hamiltonian reads

$$\widehat{H} = \hbar\omega_c \hat{a}^\dagger \hat{a} + \hbar\omega_e \hat{\sigma}^\dagger \hat{\sigma} + \hbar g(\hat{\sigma}^\dagger \hat{a} + \hat{\sigma}\hat{a}^\dagger) \quad \text{(X.5)}$$

where $\hbar\omega_c$ is the cavity mode energy and $\hbar\omega_e$ corresponds to the electronic transition energy. This Hamiltonian is written in a second quantization formalism and can be understood very intuitively. The first term represents the cavity mode, which can be treated as a harmonic oscillator. Let's recall that the ladder operators act on the Fock basis according to $\hat{a}^\dagger|n\rangle = \sqrt{n+1}|n+1\rangle$ and $\hat{a}|n\rangle = \sqrt{n}|n-1\rangle$. The second term in the Hamiltonian represents the two-level system where $\hat{\sigma}^\dagger = |e\rangle\langle g|$ and $\hat{\sigma} = |g\rangle\langle e|$, with $|g\rangle$ and $|e\rangle$ being the corresponding ground and excited state. Therefore, $\hat{\sigma}^\dagger$ acting on $|g\rangle$ creates an excitation on the two-level system while it is destroyed when $\hat{\sigma}$ acts on $|e\rangle$. Finally, the interaction between the cavity mode and the two-level system is encoded in the last term, where the coupling strength $g = 2\boldsymbol{\mu_{ge}} \cdot \boldsymbol{F_{1ph}}$, with the single-photon electric field strength $\boldsymbol{F_{1ph}}$ defined in equation X.2. It is important to remark that this interaction between the electric field $\boldsymbol{F_{1ph}}$ and the molecular transition dipole moment $\boldsymbol{\mu_{ge}}$ in the so-called strong coupling regime can modify excited-state phenomena in polaritonic chemistry. If we express this Hamiltonian within the single-excitation subspace in matrix notation, i.e. with the $\{|g,1\rangle, |e,0\rangle\}$ basis, where either the two-level system is in the ground state with one-photon in the cavity or the two-level system is in the excited state with no photon in the cavity, we get

$$\widehat{H} = \hbar \begin{pmatrix} \omega_c & g \\ g & \omega_e \end{pmatrix} \quad \text{(X.6)}$$

As we already mentioned, the onset of strong coupling depends on the intrinsic decay of the cavity mode and the molecule relative to the light-matter interaction strength. In order to account for such losses in this simplified model, an imaginary component to the energy of each constituent can be introduced as $\tilde{\omega}_c = \omega_c - i\kappa/2$

and $\tilde{\omega}_e = \omega_e - i\gamma/2$. According to these definitions, the cavity mode and molecular excited-state lifetimes τ are given by $\sim 1/\kappa$ and $\sim 1/\gamma$, respectively. By diagonalising the 2x2 Hamiltonian now with the complex frequencies $\tilde{\omega}_c$ and $\tilde{\omega}_e$, the resulting eigenstates of the system are given by $|\pm\rangle = \alpha|g,1\rangle \pm \beta|e,0\rangle$, where the amplitudes $|\alpha|^2$ and $|\beta|^2$ account for the cavity and molecular contributions. Note that if the cavity dispersion is taken into account in the Hamiltonian in equation X.6, i.e. $\hbar\omega_c(k_\parallel)$, then $|\alpha|^2$ and $|\beta|^2$, also known as the Hopfield coefficients, will depend on the in-plane wavector $k_\parallel$.

The corresponding energies once the Hamiltonian is diagonalised are given by

$$E_\pm = \frac{\hbar}{2}(\tilde{\omega}_c + \tilde{\omega}_e) \pm \frac{\hbar}{2}\sqrt{(\tilde{\omega}_c - \tilde{\omega}_e)^2 + 4g^2} \qquad \text{(X.7)}$$

By considering the situation where the cavity mode and the two-level system are in resonance at ω_0, i.e. there is zero detuning $\Delta = \omega_c - \omega_e = 0$, then the energies are given by

$$E_\pm = \hbar\omega_0 - i\hbar\frac{\kappa+\gamma}{4} \pm \frac{\hbar}{2}\sqrt{4g^2 - \left(\frac{\kappa-\gamma}{2}\right)^2} \qquad \text{(X.8)}$$

If the coupling g is larger than the molecule and cavity decay rates, then the upper and lower polaritons, $|LP\rangle = \frac{1}{\sqrt{2}}(|g,1\rangle + |e,0\rangle)$ and $|UP\rangle = \frac{1}{\sqrt{2}}(|g,1\rangle - |e,0\rangle)$ are formed with even contributions of the molecular excitation and the cavity mode.

In Figure X.7 we can easily distinguish the weak and strong coupling regimes from the energy dependence of the eigenstates as a function of the coupling strength g. For weak coupling, the real part of the energy of both the cavity mode and the excited state is degenerate (Figure X7.a), meaning that the eigenstates of the system are not significantly modified. However, the imaginary part of the energies,

representing the decay of the modes, is modified (Figure X7.b). This feature reflects the Purcell effect,[15] where the lifetime $\tau \sim 1/\gamma$ of the two-level system decreases due to the additional decay channel the cavity EM mode environment provides. This effect is clearly seen in Figure X7.d, where the excited state population decays faster for increasing coupling strength within the weak-coupling regime. For this particular example, the strong coupling regime is achieved at $g/\omega_0 \sim 0.2$ where the eigenenergies of the system split into the UP and LP, with two peaks appearing in the absorption spectrum (Figure X7.c). Moreover, the Rabi oscillations of the excited-state population can be observed in Figure X.7d when the $|e\rangle$ state of the two-level system is initially excited. Such oscillations reflect the fact that the initial bare $|e\rangle$ state is no longer an eigenstate of the system.

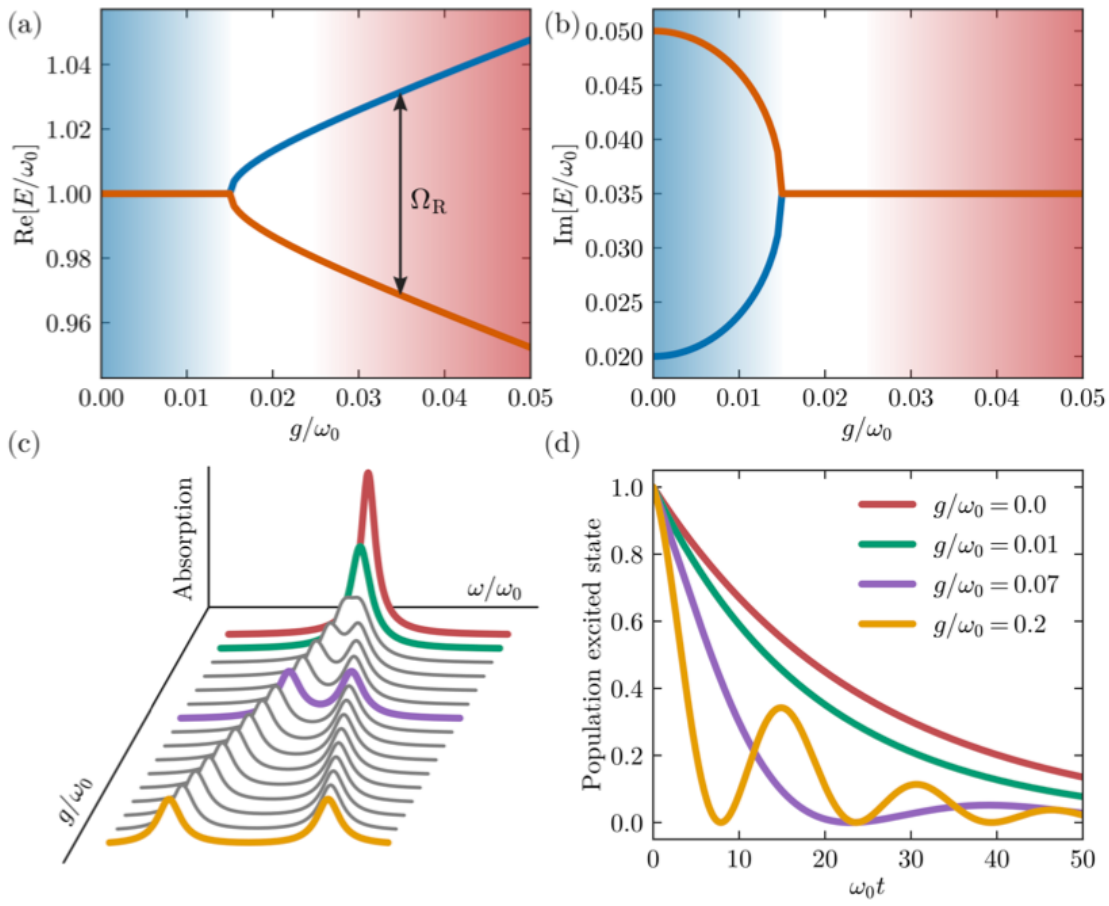

Figure X.7 A simplified model to illustrate the weak and strong coupling regimes. (a)

Real part of the eigenenergies and (b) decay rates of the eigenstates (polaritons) of the Hamiltonian as a function of the coupling strength. (c) View of the energy splitting in the absorption spectrum for different values of the coupling strength. (d) Population dynamics for the stated initiated in the molecular excited state |e⟩. The decay rates are $\gamma/\omega_0 = 0.04$ and $\kappa/\omega_0 = 0.1$.

Apart from the Jaynes-Cummings model,[49] there are other models in quantum optics describing strong coupling phenomena with additional complexity. For instance, the Tavis–Cummings model[50,51] is an extension of the Jaynes-Cummings model for the collective case where N identical two-level systems are coupled to one cavity mode. The molecular counterpart can be refined beyond the two-level system as in the Holstein–Tavis–Cummings model[52] where vibrational modes are explicitly accounted for as additional harmonic oscillators. Furthermore, these models have also been extended to the case of more than one cavity mode and are also applied to the interaction with plasmonic modes where their full spectral density can be considered.[53]

It is important to notice that when N molecules are coupled to one cavity mode in the Tavis-Cummings model, in addition to the LP and UP states, $N-1$ states appear at the bare molecular excited-state energy. These so-called dark states have no contribution from the cavity mode and are superpositions of the $|e,0\rangle$ states on different molecules.[29,54] In earlier works these were known as the exciton reservoir and they have been found to dominate the excited state dynamics in several examples.[55,56] Note that if the effect of static disorder or inhomogeneous broadening (i.e., slightly different excited state energy for each molecule) is introduced, the dark states are not degenerate anymore and will have a certain width around the bare

excited-state energy. With regard to their role in the excited state dynamics under strong coupling, it has been shown that dark states are easily populated when pumping the polaritons if the absorption band of the molecules overlaps with the polaritonic bands,[57] meaning that they are close in energy and so population can be easily transferred to them along the nonadiabatic dynamics.

Apart from quantum optics-based models where the molecular counterpart is treated as a simple two-level system coupled to a bath of harmonic modes, a more sophisticated description has also been used. Given that our intuitive understanding of chemistry comes from the Born-Oppenheimer approximation and potential energy surfaces (PES), when modelling electronic strong coupling in molecules it is very convenient to use a Jaynes-Cummings-like model where the two-level system is replaced with the molecular electronic Hamiltonian, and thus the nuclear dependence is made explicit. Next, one can perform a Born-Oppenheimer approximation for the coupled light-matter system by grouping the photonic degree of freedom with the electronic Hamiltonian.[58] This is a reasonable choice given that in electronic strong coupling, the photon energy lies within the electronic energy scale. Within this approach, strongly coupled PES are obtained, the so-called polaritonic PES (PoPES).[58,59] These have proved very useful to study photochemical and photophysical processes under strong coupling[60,61] and have also enabled the extension of already existing methods for nonadiabatic molecular dynamics simulations to investigate electronic strong coupling at the single and many-molecule level.[37,57,62–64]

In vibrational strong coupling, the transition frequencies are on the scale of nuclear vibrations and so in this situation, instead of using PoPES to study chemical modifications under VSC, a wiser strategy is to employ the so-called cavity Born-

Oppenheimer approximation (CBOA).[65,66] The general idea behind this approximation is to express the cavity mode in the Hamiltonian as an explicit harmonic oscillator, with the position and momentum operators instead of the ladder ones, and perform the CBOA treating the photonic degree of freedom as nuclear-like. In the following section we will further discuss the theory making use of the CBOA that was developed to understand VSC experiments where thermal reactions rates have been modified.[19] Given that in this chapter we mostly focus on vibrational strong coupling, we refer the interested reader to references 53, 54 and 63 for further details on applying PoPES to electronic strong coupling situations.

X.2 Polaritonic Chemistry

In this second part of the chapter we will discuss representative examples found in the literature where the rate of chemical reactions has been modified when the reactants where under strong coupling to confined light modes. We will start by briefly summarising experimental work where photochemical reactions are affected by electronic strong coupling. We will then proceed by giving an overview of experiments reporting modified thermal reaction rates under vibrational strong coupling. Regarding electronic strong coupling experiments, there are several works in the literature reporting modified photochemistry and non-adiabatic dynamics with both, Fabry-Pérot cavities and plasmonic structures,[9,68,69] and the theory of how potential energy surfaces are modified in this situation is well-established.[58,59] In contrast, although there are also numerous experiments reporting modified ground state chemistry under vibrational strong coupling,[34,70–73] the resonant and collective effects observed in these experiments are still not understood despite the theoretical attempts that have been

made, all leading to the same conclusions[19,74–76] After the survey on VSC experiments, we will describe the first theoretical attempt to understand these experiments which lead to a new proposal for modifying ground-state chemical reactions with confined light modes.[19,77]

X.2.1 Electronic strong coupling

The first experiment[68] demonstrating modified chemical reactivity under strong coupling focused on a photochromic system that consisted on a spiropyran derivative undergoing ring cleavage after UV excitation to yield the corresponding merocyanine isomer (Figure X.8a). The experiment was carried out in the solid state, where a PMMA film doped with the photochrome was embedded in a planar optical cavity (Figure X.8b). A PVA spacer was used between the silver mirrors and the PMMA film to avoid any effect of direct contact with the metal. The electronic strong coupling effects on the photoisomerization process were investigated by resonantly coupling the intense absorption band of the merocyanine product species at 560 nm to a microcavity Fabry-Pérot mode. The photochemical reaction was monitored by recording the transmission spectrum of the coupled system in the cavity (Figure X.8c), where the polariton peaks were visible once the product started to accumulate. Under strong coupling with the product's electronic transition, the photoisomerization rate from spiropyran to merocyanine was slowed down compared to control experiments in non-cavity conditions. These results showed that the molecular excited-state dynamics can be deeply affected under electronic strong coupling. After eight years one can now convincingly say that this work lead to the birth of polaritonic chemistry by raising the interest of researchers from diverse areas, ranging from nanophotonics to physical

chemistry, to investigate the potential of confined light modes to manipulate chemical properties.[31–33,59]

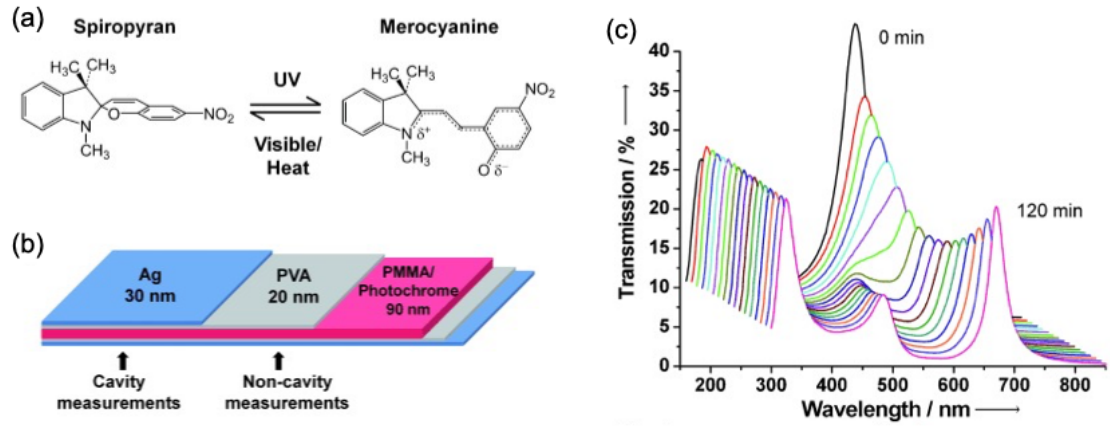

Figure X.8 (a) Spiropyran photoisomerization to merocyanine. (b) Cavity structure showing the difference between measurements under strong coupling to the non-cavity ones. (c) Transmission spectrum of the coupled system in the cavity as a function of irradiation time at 330 nm where the Ag film has a transparency window as seen in the spectra. Notice that the initial Fabry–Pérot mode at *ca.* 560 nm (black curve) splits into two new modes as the photoreaction proceeds. Reproduced from Ref. 68 with permission from Wiley-VCH, Copyright 2012.

A recent work investigating photochemistry under electronic strong coupling reported[78] the suppression of the photo-oxidation of organic chromophores by using plasmonic nanoantennas instead of planar optical cavities. Triangular silver nanoprisms were prepared in solution and their plasmonic resonance was strongly coupled to the absorption band of J-aggregates of TDBC cyanine dyes. This was possible thanks to the hybrid nanostructure of self-assembled J-aggregates on the plasmonic nanoprisms. For the experiments carried out under electronic strong coupling, the photobleaching rate of the J-aggregate dyes was significantly

suppressed and up to a 100-fold stabilisation of the organic dyes was observed when the hybrid system was red-detuned.[78] This is a very interesting result given that photobleaching is an important problem limiting the performance of optoelectronic devices since it leads to degradation of the organic chromophores. Photobleaching is usually attributed to the quenching of the dye's triplet excited state by triplet oxygen, generating singlet oxygen which is a highly reactive species. Therefore, the fact that photobleaching is suppressed under electronic strong coupling must imply that the excited state dynamics is affected by the presence of the additional polaritons and dark states that somehow prevent the organic chromophores from relaxing into their triplet state. Because plasmonic modes have very short lifetimes, of the order of a few femtoseconds, and polaritonic states in part inherit such short lifetime,[29,79] the authors concluded that the most plausible explanation to their observations is that the molecules decay faster thanks to the additional relaxation channel provided by the plasmonic nature of the hybrid excitation, and therefore, intersystem crossing (ISC) from the singlet to the triplet manifold of the dyes cannot compete because it is a much slower process. Eventually, triplet states are not efficiently populated and thus photobleaching is reduced because the molecules have already decayed to the ground state. Importantly, the photobleaching rate decreased with increasing Rabi splitting, further supporting the role of the new eigenstates of the system in the modified excited-state dynamics.

Another experimental work also investigated strong coupling effects on photochemistry,[69] focusing on the photodegradation of the semiconducting polymer 2,5-poly(3-hexylthiophene) (P3HT) (Figure X.9) commonly employed in organic photovoltaic devices. This polymer is known to photodegrade through two main mechanisms. One mechanism dominates under UV light exposure where radicals

attack the polymer causing photobleaching, while the other prevails under visible light illumination where singlet oxygen attacks the polymer. Both photodegradation mechanisms lead to a reduction and blue shift of the P3HT absorption band due to the shorter polymer chains, allowing to monitor the photodegradation process. Given that each of these two mechanisms dominates upon different spectral irradiation, the photodegradation of the P3HT polymer was thoroughly investigated with tungsten and xenon lamps, with the former emitting mostly in the visible and the latter in the UV range.

The P3HT polymer was embedded in a Fabry-Pérot cavity consisting of silver mirrors and strong coupling was achieved with a Rabi splitting of 1 eV,[69] one of the largest reported in the literature. After exposing the cavity-polymer system for several hours to tungsten and xenon lamp illumination, the polymer degradation was studied by the time evolution of the concentration of the remaining thiophene rings in the polymer. Since there are many effects at play in these experiments that can influence the reaction rate, the authors conveniently normalised the photodegradation rate considering several factors, such as for instance, catalytic effect due to direct polymer contact with the silver mirror. After these corrections they obtained a threefold reduction of the normalized rate of photodegradation under strong coupling conditions when irradiated with the tungsten lamp, when the singlet oxygen mechanism is expected to dominate. This slowing down of photodegradation is in line with the previously discussed suppression of photobleaching observed for J-aggregates with plasmonic nanocavities. The explanation the authors proposed in this work[69] was that under strong coupling, due to the Rabi splitting, the singlet-triplet gap is reduced since the LP lies below the original singlet state (Figure X.9). This leads to a reduced energy barrier for reverse intersystem crossing and thus an enhanced rate, contributing to

depopulate the triplet state that is involved in the degradation process by generating singlet oxygen. However, one must note that there is certain controversy in the literature as to whether the reverse intersystem crossing rate can be enhanced under strong coupling conditions due to the presence of numerous dark states that presumably dominate the dynamics.[55,80] Regarding the experiments with the xenon lamp illumination, the normalised photodegradation rate did not exhibit significant differences between the experiments performed in and outside the cavity, which was attributed to the absence of strong coupling in the UV spectral range.

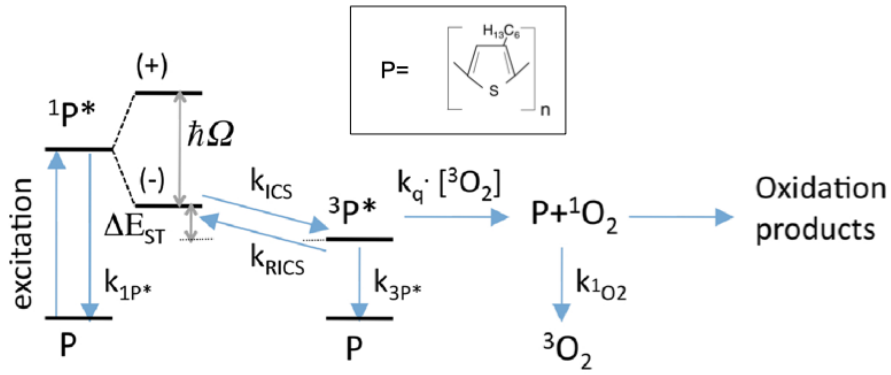

Figure X.9 Scheme of polymer photodegradation by singlet oxygen under strong coupling conditions. Legend: P, ground state of the polymer; ^{1}P* and ^{3}P*, excited singlet and triplet state of the polymer; $^3O_2$, ground state oxygen; $^1O_2$, singlet oxygen; $k_{1_{P^*}}$, k_{3*} and $k_{1_{O_2}}$, deactivation constants; k_q , quenching constant; k_r, reaction constant; k_{ISC}, intersystem crossing constant. Due to strong coupling with the cavity mode the excited state ^{1}P* is split into two polariton branches, (+) and (-). ħΩ, Rabi splitting; k_{RISC}, reverse intersystem crossing constant; ΔE_{ST}, energy difference between excited triplet state of the polymer ^{3}P* and the lower polariton branch (−) of the excited single state of the polymer ^{1}P*. Reproduced from Ref. 69 with permission from The Optical Society, Copyright 2019.

X.2.2 Vibrational Strong Coupling

X.2.2.1 Experiments

The first work that reports modification of chemical reactions under vibrational strong coupling was published in 2016.[70] The main conclusion of this work was that the rate of an organic reaction was slowed down by a factor of up to 5.5 when a vibrational mode of the reactant involved in the reaction was coupled to a microcavity mode. They investigated the S_N2 reaction shown in Figure X.10a where fluoride anions from TBAF attacked the silicon center of 1-phenyl-2-trimethylsilylacetylene (PTA) followed by protonation of the acetylide anion by methanol solvent. The experiments were carried out in an IR microfluidic cavity where the separation between the mirrors (~6 μm) was tuned so that one of the cavity modes was in resonance with an intense IR double peak at 860 cm^{-1} (Figure X.10b), attributed to the Si-C stretching mode of the reactant PTA. Since a Fabry-Pérot cavity contains a series of equally spaced resonances, a higher-order mode happened to be also in resonance with another vibration, namely, the C≡C stretching mode at 2160 cm^{-1} of PTA. The authors concluded that the Si-C mode was the only one under vibrational strong coupling according to the criterion that the Rabi splitting should exceed the widths of both the molecular transition band and the cavity resonance. However, for systems with inhomogeneous broadening for which the linewidth does not exclusively depend on the natural lifetime of the transition, significant hybridisation can be observed even when the splitting is not larger than the linewidth.

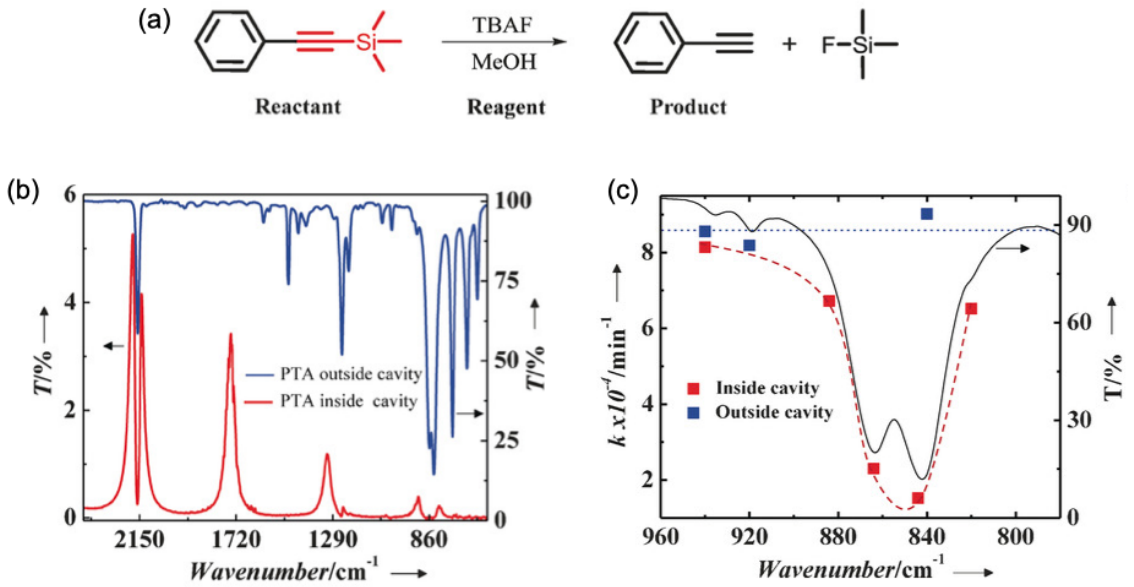

Figure X.10 (a) Studied S_N2 reaction. (b) IR transmission spectrum of the reactant (PTA) inside (red) and outside (blue) the cavity resonantly coupled to the Si-C stretching vibration at 860 cm^{-1}. (c) Reaction rate as a function of the cavity tuning for reactions inside (red squares) and outside (blue squares) the cavity. The black solid line shows the double-peaked IR absorption spectrum associated with the Si-C modes of PTA. The dotted lines are guides to the eye. Reproduced from Ref. 70 with permission from Wiley-VCH, Copyright 2016.

The evolution of the reaction was monitored by the frequency shift of a higher-order cavity mode since as the reaction evolves, the refractive index of the medium varies, causing a shift of the position of the cavity modes. This shift can then be related to the appearance of product and, by plotting this quantity over time, a linear relation was obtained indicative of an overall first-order kinetics.[70] The reaction kinetics was measured for three situations: (i) cavity on resonance with the Si-C mode, (ii) cavity off-resonance, and (iii) “outside” the cavity. The “outside” cavity control experiments were performed by replacing both cavity mirrors with dielectric windows. The rate

constant obtained for the off-resonance and outside cavity situations was the same and larger than the one obtained for the on-resonance case. The authors also found that for increasing Rabi splittings, which were obtained by increasing the PTA concentration, the quotient of the rate constant for the in-cavity vs out-cavity experiments strongly varied, with k_{in}/k_{out} ~0.4 (0.2) for Ω_R ~60 cm^{-1} (113 cm^{-1}), implying that strong coupling is indeed responsible for the modified reaction rates.

To check whether the reaction rate was only modified when the Si-C stretching vibration at 860 cm^{-1} was coupled to the cavity mode, additional experiments were carried out to verify the resonance condition in the range 820-940 cm^{-1} for the inside- and outside-cavity situations. As shown in Figure X.10c, the rate constant for the outside cavity experiments was independent of the cavity tuning, while the trend obtained for the in-cavity experiments followed the line-shape of the 860 cm^{-1} double peak. Thermodynamic quantities of the reaction were also obtained from the reaction rates determined in temperature-dependent experiments. Under VSC with a Rabi splitting of 98 cm^{-1}, $\Delta H^{\ddagger}$ increased from 9.3 to 22.9 kcal mol^{-1} and $\Delta S^{\ddagger}$ decreased from 40.9 to 1.8 eu. In a follow-up work,[81] the effects of VSC in this reaction were further investigated, in particular, the thermodynamic parameters related to the barrier were determined for different Rabi splittings. Their results showed that while $\Delta H^{\ddagger}$ and $T\Delta S^{\ddagger}$ showed significant variations with increasing Rabi splitting, given that both quantities followed the same trend, their contribution to $\Delta G^{\ddagger}$ partially cancelled out.

In the second work demonstrating modified chemical reactivity under vibrational strong coupling,[71] a very similar reaction to that investigated in the first report[70] was chosen. The difference here was that the reactant had two silicon centers instead of one (Scheme X.1). Upon nucleophilic attack with fluoride anions there were two competing S_N2 pathways in this case, related to either Si-C or Si-O cleavage, leading

to two different products, namely P_C or P_O respectively. The experimental setup was analogous to that in their first work employing a microfluidic Fabry-Pérot cavity. Several experiments were carried out under VSC to different vibrational modes of the reactant, and according to the authors, site-selective chemistry was achieved. In particular, they coupled to the Si–C and Si–O stretching modes at 842 cm^{-1} and 1110 cm^{-1}, as well as to the bending modes of the methyl groups bonded to the Si atom at 1250 cm^{-1}.

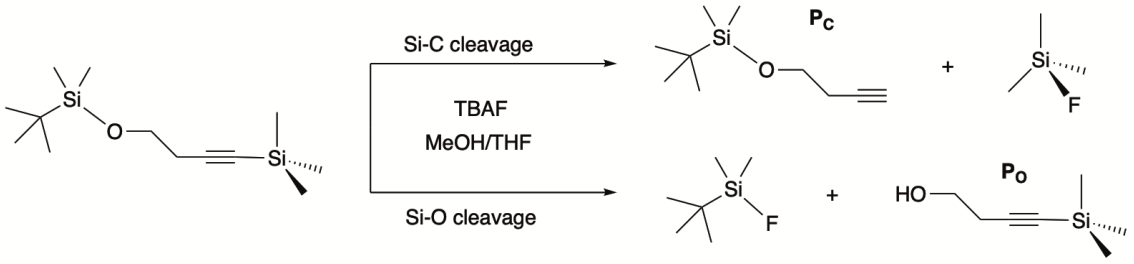

The global reaction rate was determined by measuring the temporal shift of a higher-order cavity mode, and an apparent first order kinetics was obtained. In the three VSC experiments, the reaction rate was slowed by a factor ~3, in line with their previous work. By further analysing the reaction mixture with gas chromatography–mass spectrometry, the product concentration ration $[P_C]/[P_O]$ was determined, allowing to extract the individual rate constant of the pathways involving either Si-C or Si-O cleavage. For experiments outside the cavity or those under off-resonance conditions, the product ratios were equivalent $[P_C]/[P_O]$~1.5 thus favouring the P_C product, while for the experiments under VSC either to the Si–C and Si–O stretching vibrations or to the methyl bending modes, the product ratio was inverted, favouring the P_O product with $[P_C]/[P_O]$~0.3. The individual apparent rate constants for both pathways were also estimated and temperature-dependent experiments together with transition state theory allowed to extract the corresponding activation parameters for the Si-C and Si-O cleavage routes. For the experiments under strong coupling to either

the Si–C or the Si–O stretching vibrations, the estimated $\Delta H^{\ddagger}$ and $\Delta S^{\ddagger}$ values were very similar for both the Si-C and Si-O cleavage pathways. This is indicative that there are significant limitations to the site-selectivity that can be achieved with vibrational strong coupling.

Motivated by the fact that the same product ratio was obtained for the three VSC experiments, where the cavity resonance was coupled to either the Si-C and Si-O stretching vibrations or to the bending mode of methyl groups, additional experiments were carried out, this time coupling to the C-O stretching mode of the reactant at 1045 cm^{-1}. In the IR spectrum, this transition was blurred by the broad C-O stretching band of the employed solvents, namely methanol and THF. This experiment thus provided a means to check whether the reaction rate was affected by VSC to a mode unrelated to the reaction coordinate or the solvent. As opposed to the other VSC experiments involving the Si atom and methyl groups, by coupling to the C-O stretching vibration no modification in the reaction rate nor product ratio was observed. Moreover, similarly to their previous work,[70] the reaction rate was determined for a cavity mode tuned to be resonant with several frequencies within the IR spectrum of the reactant. As shown in reference 71, a sort of resonance condition between the cavity mode and a reactant's IR peak was obtained in order to observe modified reaction rates.

Modifications of the rate of the Prins cyclization under VSC have also been reported.[73] In this reaction, either an aldehyde or a ketone reacts with an unsaturated alcohol yielding a heterocyclic product. This kind of reaction is of vital importance in synthetic routes since it allows the formation of new carbon-carbon bonds.[82] The reaction in Scheme X.2 was studied in the presence of iodine, where the cyclization between 3-butene-1-ol and two aldehydes (acetaldehyde and propionaldehyde) and

ketones (acetone and cyclohexanone) was investigated. A microfluidic Fabry-Pérot cavity was used to achieve strong coupling with the C=O stretching vibration of either the aldehyde or the ketone reactant, which was verified by angle-dependent transmission spectra where the dispersion of the lower and upper polariton branches was observed. Like in previous works, the reaction was monitored by the shift of higher-order cavity modes due to the change of refraction index of the reaction mixture as the product appeared. The reaction was found to follow a second order kinetics and the rate was determined by monitoring the reduction of the 3-butene-1-ol reactant by means of gas chromatography-mass spectrometry.

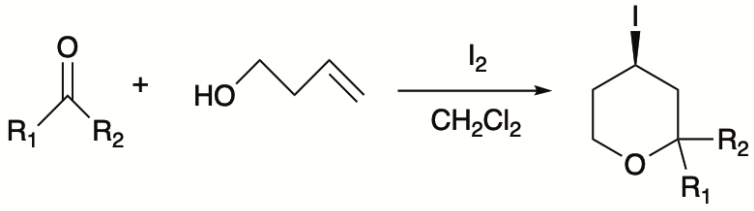

1 R_1=Me, R_2=H **3** R_1=Me, R_2=Me
2 R_1=Et, R_2=H **4** R_1-C-R_2=cyclohexane

The reaction rate under VSC conditions was slowed down for the four studied Prins cyclizations, in a similar manner to the previously reported slow-down of S_N2 reactions in VSC. In particular, the reaction rate decreased by 70% compared to the reaction carried out in off-resonant conditions, where the cavity mode was detuned from the carbonyl stretching frequency. The activation parameters for the Prins cyclization with the four considered reactants were obtained from Eyring plots of temperature-dependent experiments. The activation enthalpy in all the cases was found to increase by ~2 kcal mol^{-1} under VSC to the carbonyl group of the reactant, compared to reactions carried out in off-resonance conditions. This represented a 1.5-fold increase in the activation enthalpy, however, the entropy of activation did not suffer significant modifications under VSC. This is in contrast with the previously

reported S_N2 reactions where both the enthalpy and entropy of activation were significantly modified under VSC, as previously discussed.[70,71]

The authors found a linear correlation between the enthalpy and entropy of activation for the on-resonance and off-resonance experiments with the four reactants.[73] This led them to conclude that under VSC, the reaction pathway is not modified for either of the reactants and that the effect of VSC with the carbonyl stretching bond is to increase the activation energy barrier. Furthermore, the resonance requirement between the C=O stretching of the carbonyl group of the reactant and the cavity mode to slow-down the rate of the Prins cyclization was confirmed by determining the reaction rate in the vicinity of the carbonyl stretching vibrational frequency. Finally, the authors concluded that given that the rate-limiting step of the Prins cyclization involves the protonation of the carbonyl group and its polarity facilitates this step, then possibly the observed increase under VSC of the activation barrier is due to a decrease of the carbonyl group polarity when its stretching frequency is under VSC with the cavity mode.[73]

In the experiments we have discussed so far the reaction rate was slowed down under VSC conditions. However, catalytic VSC effects have also been observed, especially when coupling to the solvent. The first example of catalysis with VSC was reported in 2019,[34] where ester hydrolysis in basic conditions was catalysed by cooperative VSC of reactant and solvent molecules. In this reaction shown in Figure X.11a, nucleophilic attack of fluoride anions on the ester carbon of the reactant para-nitrophenyl acetate (PNPA) lead to the product para-nitro phenoxide (PNP^-), with ethyl acetate (EtOAc) as the solvent medium. A microfluidic Fabry-Pérot cavity analogous to that used in previous VSC experiments was tuned to achieve strong coupling with the C=O stretching vibration of both the reactant PNPA and the solvent EtOAc. In all

the experiments, the reactant PNPA was in excess with respect to fluoride leading to a pseudo-first-order kinetics. In order to explore whether the solvent alone could catalyse the reaction under VSC, the reaction mixture consisted of only 0.1 wt % of PNPA. Due to this negligibly small quantity of reactant compared to the solvent, the solvent was the only species under VSC during the experiments. The C=O stretching vibration at 1750 cm^{-1} was coupled to the tenth cavity mode, splitting the band into the lower and upper polaritons with a Rabi splitting of 155 cm^{-1}. In contrast to previous experiments, in this case the reaction was monitored through the appearance of the intense absorption band of the PNP^- product at 407 nm.[34]

The apparent rate constant observed under VSC to the solvent C=O stretching vibration was found to be $2.5 \cdot 10^{-2}$ s^{-1}, more than one order of magnitude larger than the rate obtained for the non-cavity experiments, $0.2 \cdot 10^{-2}$ s^{-1}. This is a clear indication that VSC of the solvent alone is able to catalyse the reaction. The authors performed further control experiments showing that the non-cavity reaction kinetics was exactly the same as the one obtained for experiments in the cavity under off-resonance conditions, demonstrating that the sole presence of the mirrors was not responsible for the observed catalysis in the VSC experiments. Moreover, in Figure X.11b,c one can clearly see that the modified reaction rates under VSC follow the C=O band envelope.

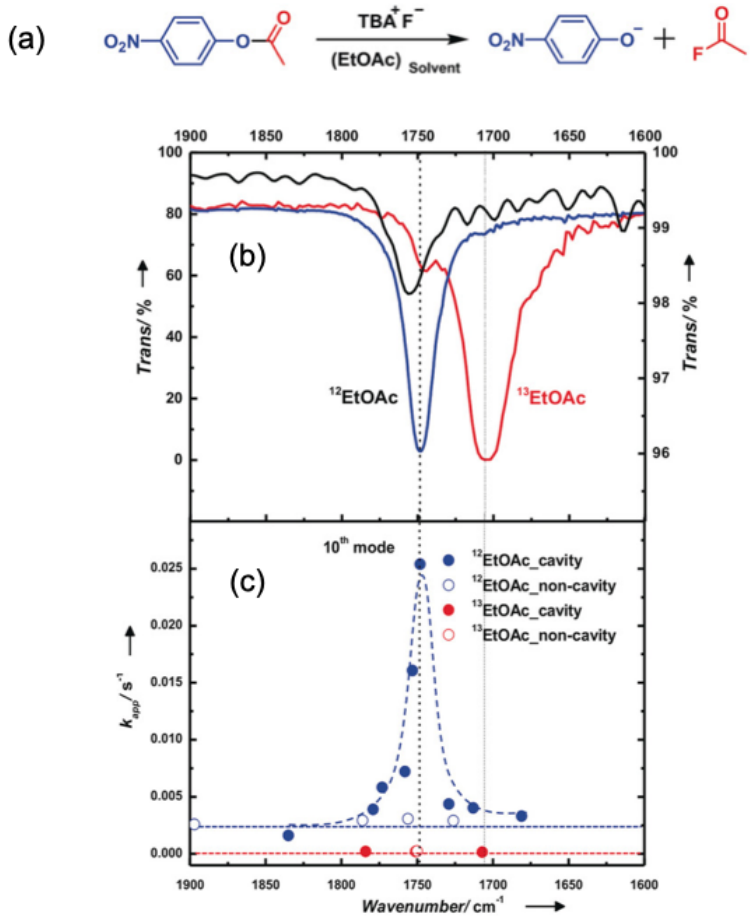

Figure X.11 (a) Hydrolysis of PNPA in ethyl acetate (EtOAc) . (b) Carbonyl stretching modes of pure PNPA (ATR spectrum; black trace); FTIR spectra of ^{12}EtOAc (blue trace) and ^{13}EtOAc (red trace) at 10 % in hexane. (c) Corresponding kinetic traces measured by tuning the cavity (^{12}EtOAc: blue filled circles; ^{13}EtOAc: red filled circles) and non-cavity (^{12}EtOAc blue empty circles; ^{13}EtOAc red empty circles); tenth mode of the cavity overlapping with the carbonyl stretching mode of ^{12}EtOAc and PNPA. The dashed curves are guides to the eye. Reproduced from Ref. 34 with permission from Wiley-VCH, Copyright 2019.

Further experiments were carried out considering the kinetic isotope effect by changing the solvent from EtOAc with ^{12}C=O to ^{13}C=O, with the stretching mode now

at 1706 cm^{-1} instead of 1750 cm^{-1}. As shown in Figure X.11c, while for the non-cavity experiments the reaction with ^{13}EtOAc is slower than with ^{12}EtOAc, possibly due to a secondary kinetic isotope effect according to the authors,[34] the reaction rate is not modified in the cavity experiments when the cavity mode is tuned to be resonant either with the ^{12}C=O or ^{13}C=O stretching modes. This is an indication that there is some cooperativity between the C=O of the reactant and the solvent, given that only when they are both at the same frequency in the ^{12}EtOAc experiments, the reaction is catalysed.[34]

Temperature-dependent experiments were carried out to obtain the thermodynamic parameters of the reaction by fitting the data to the Eyring equation. The activation enthalpy $\Delta H^{\ddagger}$ was found to decrease from 12.7 kcal mol^{-1} to 1.9 kcal mol^{-1} and the activation entropy $\Delta S^{\ddagger}$ also decreased from -16.9 eu to -49.3 eu. This resulted in a ~1 kcal mol^{-1} lower Gibbs free energy of activation under VSC conditions. Finally, experiments with varying solvent concentration were carried out and the rate was found to increase with the Rabi splitting, which, together with the results obtained in the kinetic isotope effect experiments led the authors to conclude that some cooperative effect between the reactant and the solvent must be at play given that when VSC is achieved for the C=O stretching vibration of the solvent, the reaction rate is modified compared to the non-cavity situation only when the reactant C=O stretching mode overlaps that of the solvent.[34]

Apart from this previous example where a common organic reaction was catalysed under vibrational strong coupling conditions with the solvent, a very recent work explored how this could affect the activity of a biomolecule.[83] In this case, enzymatic activity was slowed down when the water medium was under VSC with a cavity mode, in contrast to the previous example where coupling to the solvent

accelerated the reaction. The enzyme used in the experiments was pepsin which is found in the gastric juice and whose role is to digest proteins, breaking them into amino acids.[84] The authors were motivated to study pepsin's activity under VSC to water because this enzyme is a hydrolase, that is, it uses water to break chemical bonds, and moreover, water is itself the medium in which the protein folds. In the catalytic mechanism, residues in the active site activate a water molecule to act as a nucleophile, and a Michaelis–Menten kinetics is followed where in a first step the substrate binds to the enzyme and in a second one the chemical reaction takes place.[83]

In the VSC experiments realised with a microfluidic Fabry-Pérot cavity, two IR absorption bands of water were considered, the OH stretching mode at 3367 cm^{-1} as well as the bending vibration at 1642 cm^{-1}. In the case of the OH stretching mode, a Rabi splitting of 703 cm^{-1} was achieved (Figure X.12a), representing ~20% of the bare vibrational frequency, a signature that the system had reached the ultrastrong coupling regime, which was further supported by the better fit of the polariton branches obtained with an ultrastrong coupling model of coupled oscillators.[83] Interestingly, recent molecular dynamics simulations[85] of liquid water under VSC have captured the asymmetric Rabi splitting observed in the IR spectrum (Figure X.12a). Note that the enzyme, substrate and buffer were in very low concentrations in the reaction mixture, and therefore the only species under strong coupling with the cavity mode was water. In contrast to previous works on VSC modifications of chemical reactivity, in this case angle-dependent dispersion measurements were provided for the lower and upper polariton branches, where the cavity was tuned at $k_{\parallel} = 0$.

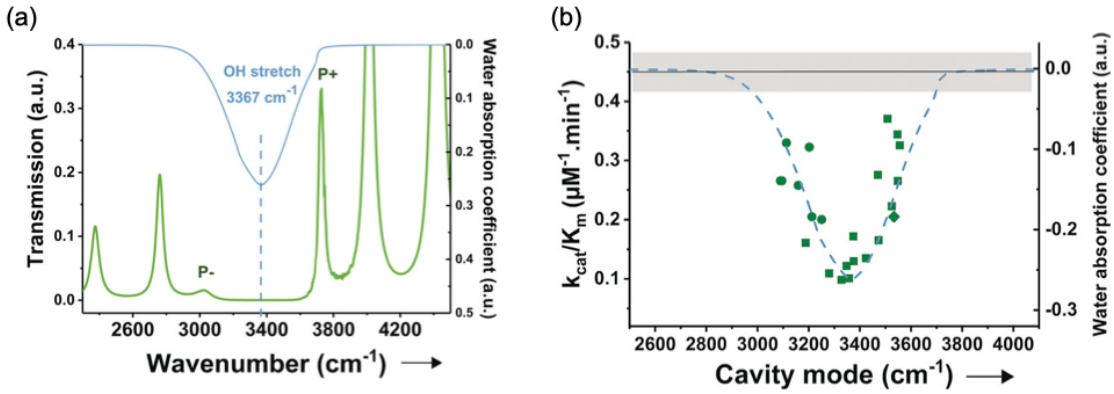

Figure X.12 (a) IR transmission spectrum of a cavity containing the reaction mixture with pepsin under vibrational strong coupling of the water OH stretching mode. Overlay with the water absorption coefficient (i.e. the imaginary part of the complex refractive index; light blue curve). (b) Pepsin enzymatic activity under vibrational strong coupling of the water stretching mode: Detuning curve of the initial velocities of the substrate digestion. Green circles: 6th order mode coupled. Green squares: 7th order mode coupled. Green diamond: 10th order mode coupled. Blue dashed curve: water absorption coefficient. Black line: average measured initial reaction velocity of reactions measured in a cell. Grey area: mean ± standard deviation of measurements in a cell. Reproduced from Ref. 83 with permission from Wiley-VCH, Copyright 2019.

The enzyme activity on a specifically designed substrate was investigated and the reaction was followed by monitoring the fluorescence band which was initially quenched and restored along the enzymatic catalysis. By coupling to the OH stretching band of water, the enzymatic activity of pepsin was slowed down by a factor of 4.5, and, moreover, when the cavity was detuned from the OH band maximum frequency, the apparent second order rate constant k_{cat}/K_m followed the shape of the IR band of the OH stretching vibration of water, as shown in Figure X.12b. However,

no modifications on the enzymatic kinetics were observed when the cavity mode was under strong coupling with the bending vibration of water.[83]

Further reactions have reported catalysis under VSC to the solvent.[86] In particular, the hydrolysis of cyanate ions with either water or deuterated water, $2H_2O$ ($2D_2O$) + $OCN^- \rightarrow CO_3^{2-} + NH_4^+$ (ND_4^+), was investigated with the OH (OD) stretching vibration coupled to a Fabry-Pérot microcavity mode. Under ultrastrong coupling conditions, the apparent rate constant increased by more than one order of magnitude either with water or deuterated water. In addition, the hydrolysis of ammonia borane, $2H_2O + NH_3BH_3 \rightarrow NH_4^+ + BO_2^- + 3H_2\uparrow$, was also investigated. When coupling to the OH stretching vibration of water in the ultrastrong coupling regime, the reaction rate was enhanced by four orders of magnitude.

Besides the modification of chemical reactions with VSC, a very recent work has demonstrated its ability to alter the equilibrium of charge-transfer complexes.[72] In particular, the equilibrium constant was either increased or decreased depending on the symmetry of the molecular vibrations strongly coupled to cavity modes. With a microfluidic Fabry-Pérot cavity setup, the complexation of mesitylene with iodine was investigated (Figure X.13). The UV spectrum of this system possesses intense bands due to charge-transfer transitions between the donor unit, mesitylene and the acceptor, iodine. From the change in absorbance of such UV bands, the Benesi–Hildebrand method was employed to obtain the equilibrium constant K_{DA} of the charge-transfer complexes. This is a typical method employed to study the equilibrium of weakly-bound systems, where apart from the equilibrium constant, the absorption coefficient ε_{DA} can also be determined from a linear plot.[87]

In this work,[72] experiments were carried out under VSC to several vibrations of mesitylene belonging either to the E' or A' irreducible representations (Figure X.13) to explore whether the symmetry of the modes can affect the complexation equilibrium. For the non-cavity case, K_{DA} was found to be 0.40 while when three distinct A' modes at different frequencies (Figure X.13a) were in VSC, K_{DA} was reduced to a value of 0.09-0.16. On the contrary, when two distinct E' modes of mesitylene (Figure X.13a) were strongly coupled to the cavity mode, K_{DA} increased with respect to the non-cavity case up to values of 1.01-1.03. This is a very interesting result showing that depending of the symmetry of the vibrational mode, the equilibrium of the complexation may be shifted to one side or the other. Moreover, the observed modifications of K_{DA} are independent of the frequency of the coupled mode, and exclusively depend on the symmetry of the irreducible representation they belong to.[72]

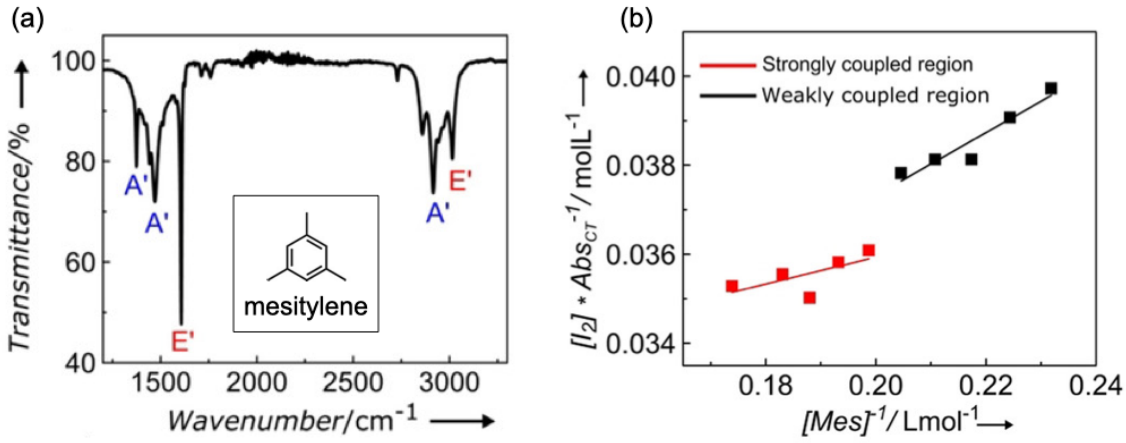

Figure X.13 (a) IR spectrum of mesitylene with the symmetry of the different vibrational modes. (b) Benesi–Hildebrand plot for the weak to strong coupling regimes when the cavity is resonant with the E' vibration at 3017 cm^{-1}. Reproduced from Ref. 72 with permission from Wiley-VCH, Copyright 2020.

In the Benesi–Hildebrand plots shown in Figure X.13b, the absorbance of the CT band multiplied by the initial concentration of iodine is plotted vs the inverse concentration of mesitylene, and K_{DA} is estimated from the slope of the linear plot. For the complexation reaction, two clearly distinct regions were observed in this plot, one at low mesitylene concentrations corresponding to a given equilibrium situation when strong coupling was not reached, and one at higher concentrations with a different slope, indicating a modified K_{DA} when the system was under VSC. Moreover, the equilibrium situation was not modified when varying the mesitylene concentration and thus the Rabi splitting in the strong coupling region. Another result suggesting that the observed modifications under VSC are exclusively due to the symmetry of the molecular vibration is the fact that very similar K_{DA} values were obtained for deuterated mesitylene compared to the original undeuterated mesitylene experiments, despite the large isotope-induced shifts in the vibrational frequencies.

Further experiments were carried out to corroborate all the previous observations. In particular, the complexation of benzene with iodine was also studied and for VSC experiments with benzene modes of E_{1u} symmetry, analogous results were obtained to those for the complexation of mesitylene with iodine under VSC to E' vibrations of mesitylene. Additional experiments under VSC to the solvent heptane were also performed but the complexation equilibrium was not modified in this case. From the Benesi–Hildebrand plots, ε_{DA} at 330 nm of the UV absorption band was also determined, and significant changes were observed only under VSC to A' vibrations. This result suggests that the symmetry of the molecular vibration under strong coupling governs the equilibrium by modifying the charge-transfer complex conformation, given that different conformations will have different oscillator strengths for the CT absorption band.[72] Finally, from temperature-dependent experiments, ΔG^{o}

of complexation was determined. For the non-cavity experiment the obtained value was 0.5 kcal mol^{-1}, while under VSC to A' modes it increased up to 1.4 kcal mol^{-1} while under VSC to E' modes it was modified on the opposite direction to 0.02 kcal mol^{-1}.

To conclude this section on VSC experiments, let us briefly mention a very interesting strategy to electrochemically switch an organic redox couple within an optical cavity.[88] The benzoquinone/dihydroquinone (BQ/dHQ) redox couple[89] (Figure X.14) was chosen given that the oxidized species BQ has a strong IR peak at 1656 cm^{-1} due to the stretching mode of the two carbonyl groups, which is absent in the reduced dHQ species. Moreover, modifications of electron-transfer rates under VSC have been theoretically predicted[90] and this redox couple has been extensively studied in terms of Marcus−Hush electron transfer theory.[91] The experimental setup consisted of a Fabry-Pérot microcavity where one of the gold mirrors acted also as working electrode. The separation between mirrors was tuned so that VSC was achieved with the symmetric carbonyl stretching vibration and the electrochemical reaction was monitored in-situ with IR spectroscopy. Under suitable biases, a solution of BQ was reduced to dHQ, leading to the electrochemical modulation of VSC where a 30 cm^{-1} Rabi splitting of the BQ species completely disappeared after full conversion to the reduced species (Figure X.14). Although the performance of the electrochemical switching deteriorated over repeating cycles, which was attributed to compositional changes of the medium, this study provides the initial grounds for future investigations of electron transfer under VSC.

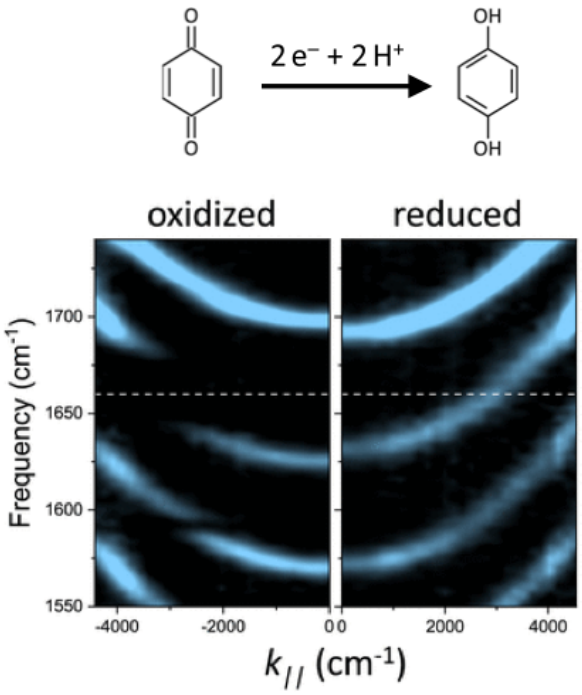

Figure X.14 Top: Scheme of species under oxidized (BQ) and reduced (dHQ) conditions. Bottom: Influence of BQ redox state on cavity dispersion. (Left) 0.3 M BQ in a ~50 μm cavity converts to its reduced state, dHQ, when held at a reducing bias (right). The anticrossing occurring at the carbonyl stretch frequency (white dashed line) is completely eliminated for the reduced form. Reproduced with permission from Ref. 88. Copyright 2020 American Chemical Society.

X.2.2.2 Theory

In the previous section we have discussed recent experiments where the rate of thermal reactions was modified under vibrational strong coupling conditions. Herein we will focus on the theory developed by our group to understand how potential energy surfaces are modified under VSC. Let us mention that apart from the effects of VSC on adiabatic chemical reactions involving the breaking and formation of covalent chemical bonds, the effect on nonadiabatic reactions has also generated interest in

the community. In particular, the catalysis of electron transfer reactions of Marcus type has been theoretically investigated both in the strong and ultrastrong coupling regimes.[90,92] Although promising results were obtained for experimentally-feasible parameters of the studied model, a recent work has pointed out that if the dispersion of the cavity mode is taken into account, thus affording a realistic description of experimental setups employed in VSC experiments where typically a Fabry-Pérot microcavity is used, then the predicted resonant catalysis of electron transfer reactions would not be observable due to the low density of states of polaritons.[93]

Motivated by all the experimental results discussed in the previous section where chemical reaction rates were modified under VSC conditions, our group pursued a thorough theoretical study to understand how potential energy surfaces are modified under VSC and what is the explicit role played by the polaritonic states.[19] Although we found that coupling cavity modes to molecular vibrations leads to modified PES of the coupled light-matter system, these modifications arise independently of whether the cavity mode is in resonance with any specific molecular vibration. In other words, according to our theory, strong coupling is not a requisite to observe modified reaction rates, in contrast to the experimental observations of chemical reactions under VSC.[70,71] Specifically, our work provides an alternative approach to modify chemical reactions with quantised light modes, which is in close relation to Casimir-Polder forces, as we will explain below. Our work can also be viewed as a theoretical framework to retrieve the interaction between metal surfaces and molecules in heterogeneous catalysis, with the novelty that such interaction can be enhanced with plasmonic nanostructures, a platform commonly used in nanophotonics but overlooked in heterogeneous catalysis. In the following lines within this section we review the main points of our investigation in a qualitative way, avoiding

the excessive use of equations in order for the general reader to capture the essence of our results. Before proceeding, we would like to point out that at the present time, the VSC experiments modifying chemical reactivity are still not understood within a rigorous theoretical framework,[19,74–76] so that there is still plenty of room for further investigations to understand the effect of vibro-polaritons in chemical reactivity.

To tackle the situation of ground state chemical-reactivity changes under vibrational strong coupling we first considered the interaction between molecules and cavity modes within the quasistatic approximation. This approximation neglects the transversal component of the electromagnetic fields, meaning that retardation effects are ignored. This is an accurate approximation when the distances of the studied system are smaller than the relevant wavelengths, as it is the case for plasmonic nanocavities where the field concentration is sufficiently enhanced to achieve strong coupling at the single-molecule level. Within this framework and considering the point-dipole approximation, we derived a Hamiltonian which allowed us to investigate the effects of VSC on the chemical kinetics of a simplified molecular model. We first considered the situation of VSC of a single molecule with a single cavity mode. The Shin-Metiu model[94] was used to represent the molecule via one-dimensional PES where the ground state consisted of two potential wells connected by a barrier mimicking the reactants and products of a chemical reaction (Figure X.15a). Since a priori it was unknown if transition state theory would hold for the reaction under vibrational strong coupling, this simplified molecular model proved very useful because it allowed the calculation of quantum reaction rates where transition state theory was not assumed.

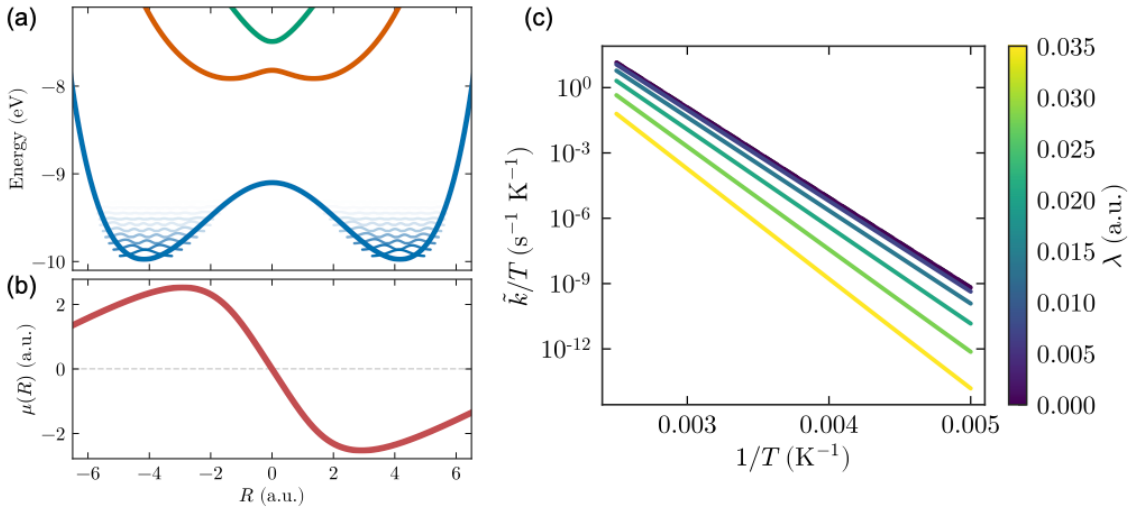

Figure X.15 (a) Potential energy surfaces of the Shin-Metiu model together with the electronic ground-state vibrational levels and corresponding probability densities (blue curve). (b) Ground-state dipole moment profile. (c) Arrhenius plot for the rate dependence with the temperature in the hybrid system for several light-matter coupling values. See the main text for details. Reproduced from Ref. 19 under the terms of the Creative Commons Attribution License CC BY 4.0 (https://creativecommons.org/licenses/by/4.0/legalcode), Copyright 2019.

The results of the quantum rate calculations of the Shin-Metiu model for a cavity mode coupled to the vibrational mode are shown in Figure X.15c, where the Arrhenius plot for different coupling strengths λ is represented. The linear plots indicate that under strong coupling to a cavity mode, there is an effective energy barrier confirming the validity of transition state theory. Moreover, the slope changes for increasing coupling strengths indicate that this barrier is modified under VSC. Therefore, in order to exploit transition state theory to understand how reaction barriers are modified under strong coupling, a strategy based on potential energy surfaces was pursued. In particular, the cavity Born-Oppenheimer approximation[65,66] (CBOA) was applied to

obtained combined photonic-nuclear potential energy surfaces, providing a useful and general framework to understand how the energy landscape is modified under strong coupling.

The main idea of the CBOA is to treat the cavity mode similarly to a nuclear degree of freedom. In order to do so, the harmonic oscillator Hamiltonian is written in terms of the position and momentum operators given by $\hat{p} = i\sqrt{\omega_c/2}(\hat{a}^\dagger - \hat{a})$ and $\hat{q} = 1/\sqrt{2\omega_c}(\hat{a}^\dagger + \hat{a})$ i.e.,

$$\hbar\omega_c\left(\frac{1}{2} + \hat{a}^\dagger\hat{a}\right) = \frac{\hat{p}^2}{2} + \frac{1}{2}\omega_c^2\hat{q}^2 \tag{X.9}$$

so that its "kinetic" and "potential" energy appear explicitly. Then, by treating the cavity mode as a nuclear degree of freedom, its kinetic energy is grouped with that of the nuclei. Note that this is a sensible choice given that in VSC, one aims to couple cavity modes to nuclear vibrations, and so their motion will be *equally slow* compared to the electronic one. Note that this is opposite to the common approach in electronic strong coupling where polaritonic PES are obtained by grouping the cavity degree of freedom with the electronic Hamiltonian.[58] After performing the standard Born-Oppenheimer approximation, the following "electronic" Hamiltonian for the coupled light-matter system is obtained,

$$\widehat{H}_e(\widehat{\boldsymbol{x}}; \boldsymbol{R}, q) = \widehat{H}_e(\widehat{\boldsymbol{x}}; \boldsymbol{R}) + \frac{1}{2}\omega_c^2 q^2 + \omega_c q\boldsymbol{\lambda}\cdot\widehat{\boldsymbol{\mu}}(\widehat{\boldsymbol{x}}; \boldsymbol{R}) \tag{X.10}$$

which depends parametrically on both the photonic q and nuclear $\boldsymbol{R}$ coordinates. Here, $\widehat{\boldsymbol{x}}$ refers to the electronic coordinate operators. The first term of this Hamiltonian is the common electronic Hamiltonian including the kinetic energy of the electrons and the nucleus-nucleus, nucleus-electron and electron-electron interaction potentials, while the second term corresponds to the potential energy of the cavity mode. The third term

stands for the interaction between the molecular dipole moment and the electric field of the cavity mode, where the coupling strength $\boldsymbol{\lambda} = \lambda\boldsymbol{\epsilon}$ is defined in equation X.3 and $\boldsymbol{\epsilon}$ is the polarisation vector. Once this Hamiltonian is diagonalised, a set of electronic CBOA potential energy surfaces is obtained, which depend parametrically on both the photonic q coordinate and the nuclear ones $\boldsymbol{R}$. In other words, the PES of the system under strong coupling are analogous to those for the bare case but with an additional nuclear coordinate which represents the cavity mode. In particular, for "pure" ground-state reactions, only a single PES plays a role, and the influence of the quantized cavity modes is fully captured by simply extending the dimensionality (i.e., the number of coordinates treated parametrically). As already shown,[19] this Hamiltonian can be straightforwardly extended to the case of coupling to several cavity modes, where the second and third terms of the Hamiltonian would be replaced with $\frac{1}{2}\sum_k \omega_k^2 q_k^2$ and $\sum_k \omega_k q_k \boldsymbol{\lambda}_k \cdot \hat{\boldsymbol{\mu}}(\hat{\boldsymbol{x}}; \boldsymbol{R})$, with k labelling the distinct cavity modes.

By applying this approach to the Shin-Metiu model, potential energy surfaces within the CBOA were obtained.[19] In Figure X.16a the two-dimensional ground state PES is shown, which depends on the nuclear $\boldsymbol{R}$ degree of freedom and the cavity q one. By finding the minimum energy path along q, the one-dimensional PES in Figure X.16b was obtained for different coupling strengths. Here one clearly sees that the energy barrier increases with increasing coupling strength, in line with the previous results from the quantum rate calculations. However, the CBOA provides further physical insight given that with the PES of the coupled light-matter system one can clearly see that the modified barrier is due to stabilization of the reactant with increasing coupling strength. Furthermore, the Shin-Metiu model served as a benchmark to validate the use of transition state theory with the energy barrier extracted from the CBOA PES against the quantum rate calculations. More

specifically, the effective energy barriers extracted from the Arrhenius plots of the quantum rate calculations in Figure X.15c were compared to those from the CBOA PES. These results are shown in Figure X.16c for a wide range of coupling strengths, where an excellent agreement between both energy barriers is obtained once the zero-point energy is taken into account. In accordance with these results, the ratio between the reaction rate under VSC obtained from either transition state theory or the quantum rate calculations to that of the bare reaction perfectly overlaps for the whole range of considered coupling strengths, supporting the use of the CBOA potential energy surfaces to study molecules coupled to cavity modes.

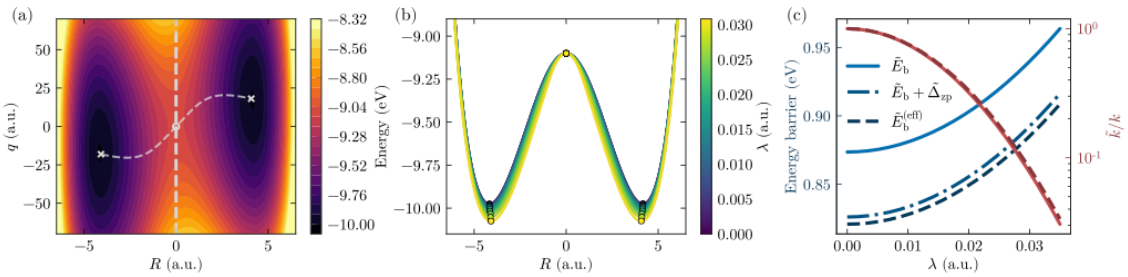

Figure X.16 (a) Two-dimensional ground-state PES within the cavity Born-Oppenheimer approximation for the Shin-Metiu model (λ=0.02 a.u., and ω_c=72.6 meV). The grey dashed curve connecting the two minima corresponds to the energy path along the minimum in the photonic coordinate q. (b) Energy profile along the minimum of q for different values of the coupling strength. (c) Energy barrier and ratio between the reaction rate under strong coupling, $\tilde{k}$, and that for the normal situation (i.e. $\lambda = 0$), k, versus the coupling strength. Results are shown for the case of barriers that were extracted from the CBOA PES (full lines) as well as that where effective barriers were fitted from exact quantum rate calculations (dashed lines). Reproduced from Ref. 19 under the terms of the Creative Commons Attribution License CC BY 4.0 (https://creativecommons.org/licenses/by/4.0/legalcode), Copyright 2019.

Acknowledging the usefulness of transition state theory within the CBOA, a further step was taken in order to obtain an explicit expression for the modified potential energy surfaces. Within perturbation theory up to second order in λ, for the case of coupling to several cavity modes, the energy shift in the potential energy surface reads[19]

$$\delta E(\boldsymbol{R}) = -\sum_k \frac{\lambda_k^2}{2}\left(\mu_0^2(\boldsymbol{R}) + \frac{\omega_k}{2}\alpha_0(\boldsymbol{R})\right) \quad \text{(X.11)}$$

where μ_0 is the ground state permanent dipole moment of the bare molecule, α_0 is the ground state static polarisability, $\boldsymbol{R}$ refers to the nuclear coordinates, and for simplicity the cavity modes are assumed to be aligned with the molecular dipole. Note that this perturbation theory result was found to be valid up to coupling strengths λ just above 0.02 atomic units (equation X.3), with an equivalent mode volume of 4.7 nm^3. According to this expression, when one or several cavity modes are coupled to a molecular vibration, the energy of the system is modified by an amount proportional to the ground state permanent dipole moment squared and the molecular polarizability. It turns out this is the well-known Casimir-Polder energy shift that interacting bodies experience due the quantised vacuum field.[95] These are physical forces which are a generalisation of van der Waals interactions.[6,96,97] Indeed, if one considers a small plasmonic nanoparticle approximated as a point dipole interacting with a molecule, equation X.11 retrieves their van der Waals interaction potential.[19] For this situation in particular we have shown that the first term of equation X.11 corresponds to the Debye interaction, that is, the interaction between the permanent dipole moment of the molecule and the dipole it induces in the nanoparticle, while the second term corresponds to the London interaction between fluctuating dipoles of both entities.[98,99]

This result shows that when molecular vibrations are coupled to confined light modes, strong coupling *per se* is not needed to achieve modified chemical kinetics, given that the energy shifts in equation X.11 do not depend on the VSC Rabi splitting. In other words, the presence of polaritons is not a requisite, and energy barriers are modified exclusively due to Casimir-Polder or van der Waals interactions. Furthermore, this theory was extended to the case of multiple molecules,[19] and collective effects were only found when all the permanent dipole moments were aligned with the cavity field, a condition which is not fulfilled in the VSC experiments in solution.

However, as we have already discussed in the previous section, modified chemical reactivity has been observed when cavity modes were in resonance to specific molecular vibrations and polaritons were formed. In light of this experimental result, the dependence of the reaction rate on the simplified molecular Shin-Metiu model with the full exact Hamiltonian without the CBOA was investigated by tuning the cavity mode to a broad range of frequencies.[19] In accordance with equation X.11, the reaction rate did not depend on the cavity mode frequency. Over the last year, several works have arrived to our same conclusion with respect to the formation of polaritons and modified chemical reactivity.[74–76] In addition, a very recent work reporting electronic structure calculations for the first reactions modified under vibrational strong coupling suggests a completely new assignment of the molecular vibrations that were coupled to cavity modes in the original experiments.[100]

Let us note that although the theory discussed in this section was developed for coupling to plasmonic modes, our findings regarding the non-requirement of resonance still hold for modes in optical cavities. In contrast to plasmonic modes, cavity modes are propagating photons and some authors claim that the so-called self-energy term should be considered in the Hamiltonian.[101] As we already discussed in

the original version of our manuscript,[102] the inclusion of this term leads to an expression analogous to equation X.11 where in this case, instead of the ground-state molecular dipole μ_0, the uncertainty of the ground-state dipole moment appears. In particular, μ_0^2 must be replaced by $-\Delta\mu_0^2$ where $\Delta\mu_0^2 = \langle\mu_0^2\rangle - \langle\mu_0\rangle^2$. Therefore, resonance effects are not obtained either when the self-energy term is considered. Note that this result has also been obtained very recently by another group.[74]

Focusing on our result in equation X.11, coupling to confined light modes can be exploited to modify energy barriers, and in turn chemical reaction rates, taking advantage of the enhanced electric fields in plasmonic nanocavities. The general idea is the following. For a given reaction, if the reactant and the transition state (TS) have significantly different permanent dipole moments or static polarizabilities, then one of the species will be further stabilised relative to the other when interacting with a cavity mode, leading to modified energy barriers and catalysis or inhibition of chemical reactions. Regarding the Shin-Metiu results in Figures X.15c and X.16c, we can now understand why the effective energy barrier in the Arrhenius plots increased with the coupling strength, in other words, why the minima in Figure X.16b were stabilised while the TS remained unperturbed. This is because of the profile of the permanent dipole moment shown in Figure X.15b, which is null in the TS configuration.

As we can see from equation X.11, sufficiently strong coupling strengths λ_k to the cavity modes will be needed for these modifications to be observable in experiments. For these purposes, we estimated the coupling strength of a realistic multi-mode plasmonic nanocavity.[19] We focused on a nanoparticle-on-mirror setup, for which single-molecule electronic strong coupling has been achieved.[20] Given that the contribution of the Debye force is likely to be the leading term in the energy shift of equation X.11, we calculated the change in the energy barrier of the Shin-Metiu

model by solving the electrostatic problem of having a point dipole in the gap of the nanoparticle-on-mirror cavity, as shown in Figure X.17. From this energy shift the effective coupling strength $\lambda_{eff} = \sqrt{\sum_k \lambda_k^2}$ from equation X.11 was extracted for different gaps of the nanocavity. Note that experimental realisations of electronic strong coupling experiments with a nanoparticle-on-mirror have reached a gap of ~1nm.[20] At approximately this gap value, significant energy barrier shifts are obtained for this model of up to ~1.5 kcal mol^{-1}, corresponding to a coupling strength of 0.02 a.u. (F_{1ph}~0.1-0.2 V/Å, see Textbox 3), a value for which the perturbation theory expression is still valid.[19] These results suggest that the energy shifts due to the interaction with cavity modes are significant and they also demonstrate the importance of the multimode nature of these cavities when interacting with matter.

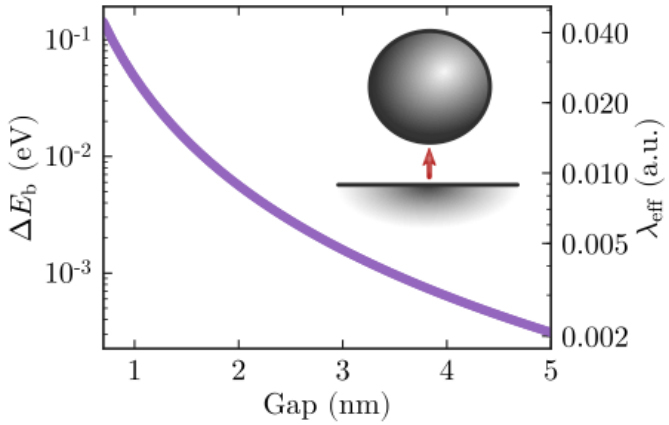

Figure X.17 Change of the energy barrier for the Shin-Metiu model interacting with a nanoparticle-on-mirror cavity as a function of the gap size. The right vertical axis shows the corresponding values of the effective single-molecule coupling strength, λ_{eff}. Inset: Illustration of the nanoparticle-on-mirror cavity geometry with a single molecule placed in the nanogap between a planar metallic surface and a small metallic nanoparticle of radius R=20 nm. Reproduced from Ref. 19 under the terms of the

Having showed that significant coupling strengths are attainable in realistic multimode nanocavities, we implemented our theory with electronic structure calculations to study how typical organic reactions can be modified by interacting with confined light modes.[77] In particular, we focused on S_N1 and S_N2 reactions, given that the permanent dipole moment of the involved species is expected to significantly vary as the reaction proceeds, leading to energy shifts in the reaction profile according to equation X.11. Furthermore, we also validated the use of this expression, which was derived from perturbation theory, by a direct optimization of the CBOA surface (equation X.10).[77]

We first studied the hydrolysis of tert-butyl chloride, which proceeds via an S_N1 mechanism.[103] Electrostatic catalysis of S_N1 reactions is also discussed in the chapters by Shaik et al. (Chapter X) and Coote et al. (Chapter X). The rate-limiting step is known to be the separation of the leaving group leading to a carbocationic intermediate, thus we focused on this first step of the reaction. In Figure X.18 we show the energy profile from reactants to the TS that leads to the carbocationic intermediate. The reaction profile was obtained with equation X.11 and in this case, the modified energetics is mainly due to the Debye interaction. We considered coupling strengths up to λ_{eff}=0.02 a.u., since as we discussed previously, realistic multimode nanocavities can reach this value.[19] As the coupling strength increases (darker), the TS is further stabilised, lowering the barrier, given that the permanent dipole moment significantly increases as the chloride leaves. By coupling to the plasmonic nanocavity

modes, the barrier is lowered by ~4 kcal mol^{-1} for the largest considered coupling strength, which is ~20% of the reaction's barrier in normal conditions.[77] The configuration of the TS is also modified due to coupling with the plasmonic modes. As shown in Figure X.18, the TS represented with blue circles shifts towards smaller C-Cl bond lengths as the coupling strength increases. In particular, for λ_{eff}=0.02 a.u., the C-Cl bond length decreases by 0.18 Å while the C-C-Cl angle increases by 13º. This trend is also observed for the TS optimised with a self-consistent electric field shown as red triangles. The good correspondence between both transition states validates the use of the perturbation theory expression with the range of coupling strengths considered. This is a very important result allowing to investigate molecules coupled to confined light modes with the simple expression in equation X.11.

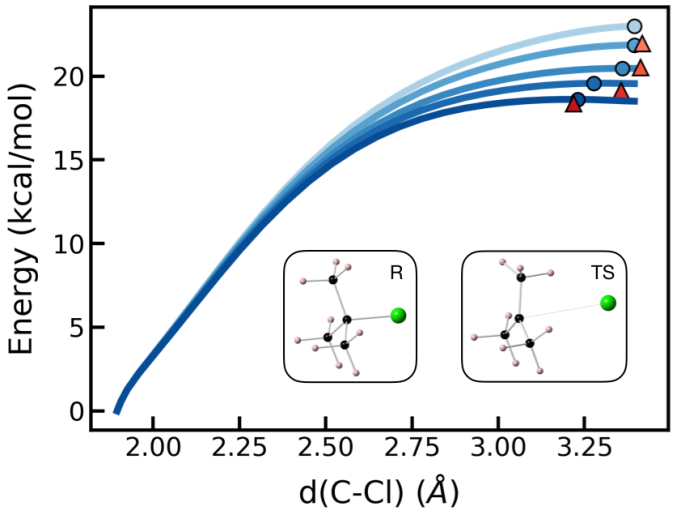

Figure X.18 Reaction profile for the initial step of the S_N1 reaction involving leaving group separation of tert-butyl chloride. Increasing colour darkness corresponds to increasing coupling strength (λ_{eff}= 0, 0.01, 0.015, 0.0175, 0.02 a.u. where the corresponding effective single-photon electric field F_{1ph}~0.1-0.2 V/Å, see Textbox 3). Blue circles correspond to the TS within perturbation theory while red triangles indicate the optimized TS obtained with a self-consistent electric field. Reactant (R) and

transition state (TS) structures are shown for the bare case (i.e. λ_{eff}= 0). Colour code: Cl green, C black. Reproduced from Ref. 77 with permission from Wiley-VCH, Copyright 2019.

The popular S_N2 Menshutkin reaction[104] was also studied under coupling to confined light modes.[77] Additional electric-field effects on this reaction are described in depth by Shaik et al. in Chapter X and in reference 105. In this reaction, ammonia attacks methyl chloride forming a pentacoordinated TS and eventually an ion-pair product complex. Since the permanent dipole moment significantly increases in the TS configuration relative to the reactants, for λ_{eff}=0.02 a.u. the energy barrier of 13 kcal mol^{-1} decreased by 20%, with an 84% contribution from the Debye interaction and the remaining 16% from the London one (Figure X.19). Therefore, in this case, the molecular polarizability also contributes to catalyse the reaction, in contrast to the previous example where the reaction modifications were exclusively due to the Debye interaction. In this example, the product is also stabilised relative to the reactants, suggesting that there may be cases where the relative forward and backward reaction rates may be modified by coupling to plasmonic modes. Furthermore, the transition state configuration is also modified in this reaction, with larger coupling strengths leading to a TS with a longer C-N bond length and a shorter C-Cl one. Again, a very nice agreement is also obtained for the full calculation and the perturbation theory results.

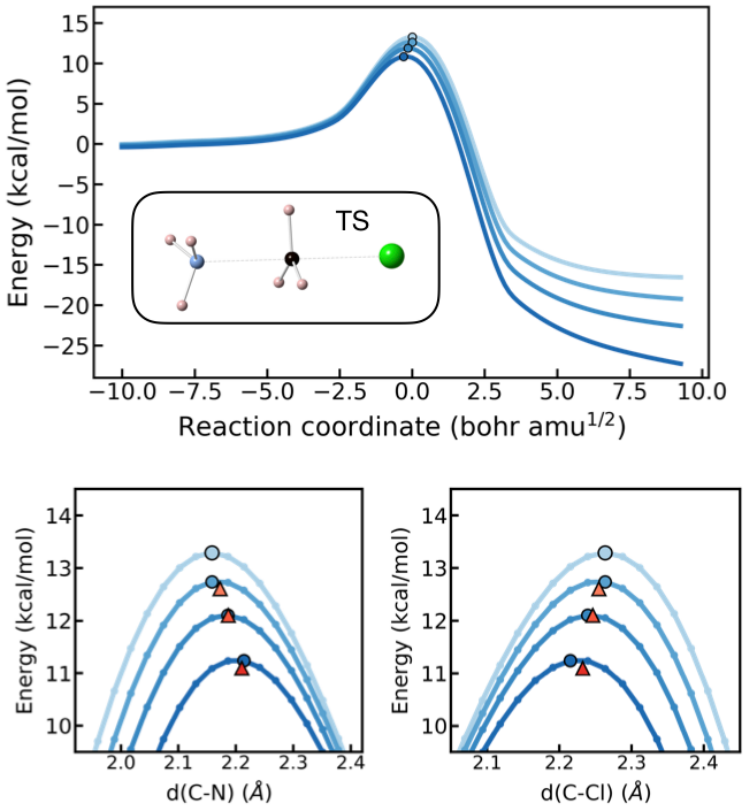

Figure X.19 Profile (top) for the S_N2 reaction. Increasing colour darkness corresponds to increasing coupling strength (λ_{eff}=0, 0.01, 0.015, 0.02 a.u. where the corresponding effective single-photon electric field F_{1ph}~0.1-0.2 V/Å). Zoom of the barrier region (bottom) plotted along the d(C-N) and d(C-Cl) bond lengths. Blue circles correspond to the TS within perturbation theory while red triangles indicate the optimized TS obtained with a self-consistent electric field. The TS geometry is shown for the bare case. Reproduced from Ref. 77 with permission from Wiley-VCH, Copyright 2019.

Given that the relative energy between two species can be modified by coupling to confined light modes, this scenario was exploited to modify the transition temperature $T_{1/2}$ of spin-crossover complexes.[77] In these systems,[106] the Gibbs free energy of a low and high spin (LS and HS) state are close enough so that depending

on the temperature, either of both spin states can become the ground state of the system. The transition temperature $T_{1/2}$ is defined such that both states are equally populated. The main idea behind this work was to use plasmonic modes to modify the relative energy of the two spin states and therefore, control the $T_{1/2}$ of these complexes, modulating their spin-crossover behaviour. In our work we considered four-coordinated Fe^{II} phosphoraminimato complexes with the general formula $PhB(MesIm)_3Fe{=}PR_3$ with R = H, Me, ^{n}Pr, Ph (Figure X.20) that undergo a spin-crossover transition in solution from a singlet to a quintet state.[107] In these complexes, a correlation between the size of the phosphine ligand and $T_{1/2}$ had been previously found.[108]

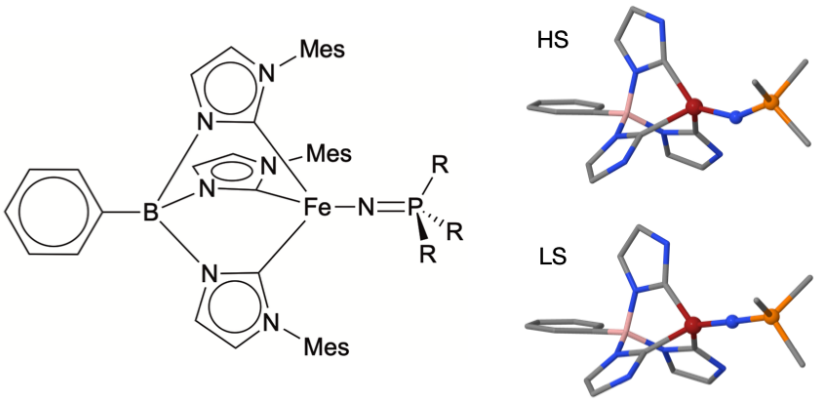

Figure X.20 Chemical structure of the Fe^{II} complexes with R = H, Me, ^{n}Pr, Ph. Crystal structure of the HS and LS states of the complex with R=Me is shown. The three Mes ligands together with all the hydrogen atoms have been omitted for the sake of clarity. Colour code: B pink, Fe brick red, N blue, P orange, C grey. The Fe-N=P fragment is shown in CPK.

According to electronic structure calculations,[77] the LS state lies 2-5 kcal mol^{-1} below the HS state, allowing a thermal transition to occur among them. In order to be

able to modify the $T_{1/2}$ of these complexes by interacting with plasmonic modes, the permanent dipole moment between the LS and HS states should be sufficiently different. Indeed, for the LS state, the permanent dipole moment is aligned along the Fe-N=P axis and is roughly 3 D larger than that of the HS state (Table X.1). The direction of the permanent dipole moment of the HS state differs from that of the LS. In particular, as shown in Figure X.20, the Fe-N=P fragment is no longer linear in the HS state and the permanent dipole moment lies along the N=P bond which is approximately 20º tilted from the Fe-N axis. In addition to the larger dipole moment of the LS state that translated into a larger energy difference between both states, the slightly different direction of both dipole moments also allows to modulate their relative energy through the polarisation of the EM mode. As shown in Table X.1, by coupling to a nanocavity mode, the $T_{1/2}$ increases 30 K on average for the four complexes with λ_{eff}=0.02 a.u. when the dipole moment of both states is aligned with the polarisation of the plasmonic mode. Even larger modifications of $T_{1/2}$ can be achieved if the permanent dipole moment of the LS state is aligned with the polarisation of the plasmonic mode and that of the HS state lies perpendicular.

Table X.1 Dipole moment for the LS and HS states of the studied Fe(II) complexes together and the experimental spin-crossover transition temperature and that estimated for λ_{eff}=0.00 and 0.02 a.u. Reproduced from Ref. 77 with permission from Wiley-VCH, Copyright 2019.

R	μ (D)			$T_{1/2}$ (K)		
	LS	HS	Exp.	0.00	0.02[(a)]	0.02[(b)]
H	4.60	2.05	-	392	417	423
Me	6.20	3.21	340	351	384	396
^{n}Pr	6.26	3.05	214	192	226	237
Ph	5.56	2.31	81	74	98	103

[(a)] μ_{HS} and μ_{LS} aligned with the polarisation of the plasmonic mode. [(b)] μ_{LS} aligned with the polarisation of the plasmonic mode and perpendicular to μ_{HS}.

The results discussed in this section demonstrate that chemical reactions as well as material properties can be modified by the coupling of molecular dipole moments with confined light modes of plasmonic structures. In this scenario, a Casimir-Polder force that depends on the nuclear coordinate is capable of modifying the energy landscape. This approach goes beyond traditional heterogeneous catalysis, exploiting the extremely enhanced electromagnetic fields in plasmonic nanostructures.

X.3 Outlook

In this chapter we have given an overview of the young polaritonic chemistry field, specially focusing on the experiments that have reported modified rates of thermal reactions under vibrational strong coupling to microcavity modes. Although new experiments showing modified chemical kinetics continue to be published, there

is still no thorough experimental work aiming to understand how vibrational strong coupling is able to modify chemical dynamics. For the field to move forward, it is essential to understand the working mechanism of vibrational strong coupling in these experiments to be able to manipulate ground-state chemical reactivity with confined light modes in a controlled manner.

As we have discussed in the last part of this chapter, motivated by these experiments, our group carried out theoretical research aiming to understand how potential energy surfaces can be modified under vibrational strong coupling. Our conclusion was that resonance between a cavity mode and a molecular vibration is not a requisite to observe modified reaction rates. Essentially, according to our theory, strong coupling is not required and therefore there are no collective effects at play. In contrast, all these experiments are done in solution in microfluidic cavities under collective strong coupling. Furthermore, as discussed in section X.2.2.1, a resonance condition between the cavity mode and molecular vibration has been obtained in several works, with the IR molecular vibration peak overlapping the reaction rates determined at different cavity detunings.

In light of the lack of a quantitative theoretical explanation for some of the experimental findings, further investigations are required. These should put special focus on the resonance requisite between cavity modes and molecular vibrations, on the role played by the solvent in vibrational strong coupling experiments, and on the symmetry of the molecular vibrations themselves. To conclude, we believe that this exciting field has a bright future ahead. There is already and we envisage that there will be an even more widespread combined experimental and theoretical effort to develop novel strategies to improve our understanding of cavity-enhanced catalysis, i.e., the modification of chemical reactivity under strong light-matter coupling.

Acknowledgement

We are extremely grateful to Dr. Javier Galego for his significant contribution to our joint investigations discussed in this chapter. This work was funded by the European Research Council through Grant No. ERC-2016-StG-714870 and the Spanish Ministry for Science, Innovation, and Universities - Agencia Estatal de Investigación through Grant Nos. RTI2018-099737-B-I00, PCI2018-093145 (through the QuantERA program of the European Commission), and CEX2018-000805-M (through the María de Maeztu program for Units of Excellence in R&D).

References

1 A. V. Kavokin, J. J. Baumberg, G. Malpuech and F. P. Laussy, *Microcavities*, Oxford University Press, Oxford, 2007.

2 C. Cohen-Tannoudji, J. Dupont-Roc and G. Grynberg, *Photons and Atoms*, Wiley, Weinheim, Germany, 1997.

3 C. I. Sukenik, M. G. Boshier, D. Cho, V. Sandoghdar and E. A. Hinds, *Phys. Rev. Lett.*, 1993, **70**, 560.

4 W. E. Lamb and R. C. Retherford, *Phys. Rev.*, 1947, **72**, 241.

5 H. B. G. Casimir, *Indag. Math.*, 1948, **10**, 261.

6 S. Y. Buhmann, *Dispersion Forces I: Macroscopic Quantum Electrodynamics and Ground-State Casimir, Casimir–Polder and van der Waals Forces*, Springer-Verlag, Berlin, 2012, vol. 247.

7 S. Haroche and J.-M. Raimond, *Exploring the Quantum*, Oxford University Press, Oxford, 2006.

8 J. T. Hugall, A. Singh and N. F. van Hulst, *ACS Photonics*, 2018, **5**, 43.

9 D. G. Baranov, M. Wersäll, J. Cuadra, T. J. Antosiewicz and T. Shegai, *ACS Photonics*, 2018, **5**, 24.

10 S. A. Maier, *Plasmonics: Fundamentals and Applications*, Springer US, New York, NY, 2007.

11 M. S. Tame, K. R. McEnery, Ş. K. Özdemir, J. Lee, S. A. Maier and M. S. Kim, *Nat. Phys.*, 2013, **9**, 329.

12 P. Törmä and W. L. Barnes, *Rep. Prog. Phys.*, 2014, **78**, 13901.

13 K. Leosson, *J. Nanophotonics*, 2012, **6**, 061801.

14 D. Sanvitto and S. Kéna-Cohen, *Nat. Mater.*, 2016, **15**, 1061.

15 E. M. Purcell, *Phys. Rev.*, 1946, **69**, 674.

16 A. Frisk Kockum, A. Miranowicz, S. De Liberato, S. Savasta and F. Nori, *Nat. Rev. Phys.*, 2019, **1**, 19.

17 J. George, A. Shalabney, J. A. Hutchison, C. Genet and T. W. Ebbesen, *J. Phys. Chem. Lett.*, 2015, **6**, 1027.

18 D. A. Steck, Quantum and Atom Optics, http://atomoptics-nas.uoregon.edu/~dsteck/teaching/quantum-optics/quantum-optics-notes.pdf%0A, (accessed 6 July 2020).

19 J. Galego, C. Climent, F. J. Garcia-Vidal and J. Feist, *Phys. Rev. X*, 2019, **9**, 21057.

20 R. Chikkaraddy, B. de Nijs, F. Benz, S. J. Barrow, O. A. Scherman, E. Rosta, A. Demetriadou, P. Fox, O. Hess and J. J. Baumberg, *Nature*, 2016, **535**, 127.

21 V. A. Yakovlev, V. G. Nazin and G. N. Zhizhin, *Opt. Commun.*, 1975, **15**, 293.

22 I. Pockrand, A. Brillante and D. Möbius, *J. Chem. Phys.*, 1982, **77**, 6289.

23 V. Agranovich, H. Benisty and C. Weisbuch, *Solid State Commun.*, 1997, **102**, 631.

24 C. Weisbuch, M. Nishioka, A. Ishikawa and Y. Arakawa, *Phys. Rev. Lett.*, 1992, **69**, 3314.

25 J. P. Reithmaier, G. Sęk, A. Löffler, C. Hofmann, S. Kuhn, S. Reitzenstein, L. V Keldysh, V. D. Kulakovskii, T. L. Reinecke and A. Forchel, *Nature*, 2004, **432**, 197.

26 F. P. Laussy, E. del Valle and C. Tejedor, *Phys. Rev. Lett.*, 2008, **101**, 83601.

27 D. G. Lidzey, D. D. C. Bradley, M. S. Skolnick, T. Virgili, S. Walker and D. M. Whittaker, *Nature*, 1998, **395**, 53.

28 D. G. Lidzey, D. D. C. Bradley, A. Armitage, S. Walker and M. S. Skolnick, *Science,* 2000, **288**, 1620.

29 M. Litinskaya, P. Reineker and V. M. Agranovich, *J. Lumin.*, 2004, **110**, 364.

30 T. W. Ebbesen, *Acc. Chem. Res.*, 2016, **49**, 2403.

31 R. F. Ribeiro, L. A. Martínez-Martínez, M. Du, J. Campos-Gonzalez-Angulo and J. Yuen-Zhou, *Chem. Sci.*, 2018, **9**, 6325.

32 M. Hertzog, M. Wang, J. Mony and K. Börjesson, *Chem. Soc. Rev.*, 2019, **48**, 937.

33 F. Herrera and J. Owrutsky, *J. Chem. Phys.*, 2020, **152**, 100902.

34 J. Lather, P. Bhatt, A. Thomas, T. W. Ebbesen and J. George, *Angew. Chemie Int. Ed.*, 2019, **58**, 10635.

35 A. Csehi, G. J. Halás, L. Cederbaum and Á. Vibók, *J. Chem. Phys. Lett.*, 2017, **8**, 1624.

36 A. Csehi, M. Kowalewski, G. J. Halász and Á. Vibók, *New J. Phys.*, 2019, **21**, 93040.

37 I. S. Ulusoy, J. A. Gomez and O. Vendrell, *J. Phys. Chem. A*, 2019, **123**, 8832.

38 M. Kowalewski, K. Bennett and S. Mukamel, *J. Chem. Phys.*, 2016, **144**, 54309.

39 B. Gu and S. Mukamel, *Chem. Sci.*, 2020, **11**, 1290.

40 A. F. Koenderink, *Opt. Lett.*, 2010, **35**, 4208.

41 M. I. Stockman, K. Kneipp, S. I. Bozhevolnyi, S. Saha, A. Dutta, J. Ndukaife, N. Kinsey, H. Reddy, U. Guler, V. M. Shalaev, A. Boltasseva, B. Gholipour, H. N. S. Krishnamoorthy, K. F. MacDonald, C. Soci, N. I. Zheludev, V. Savinov, R. Singh, P. G. C. Lienau, M. Vadai, M. L. Solomon, D. R. Barton, M. Lawrence, J. A. Dionne, S. V Boriskina, R. Esteban, J. Aizpurua, X. Zhang, S. Yang, D. Wang, W. Wang, T. W. Odom, N. Accanto, P. M. de Roque, I. M. Hancu, L. Piatkowski, N. F. van Hulst and M. F. Kling, *J. Opt.*, 2018, **20**, 43001.

42 A. Cuartero-González and A. I. Fernández-Domínguez, *Phys. Rev. B*, 2020, **101**, 035403.

43 P. A. Huidobro and A. I. Fernández-Domínguez, , DOI:2019, arXiv:cond-mat/1907.13546.

44 M. Sukharev and A. Nitzan, *J. Phys. Condens. Matter*, 2017, **29**, 443003.

45 M. L. Juan, M. Righini and R. Quidant, *Nat. Photonics*, 2011, **5**, 349.

46 W. Wang, M. Ramezani, A. I. Väkeväinen, P. Törmä, J. G. Rivas and T. W. Odom, *Mater. Today*, 2018, **21**, 303.

47 J. M. Winkler, F. T. Rabouw, A. A. Rossinelli, S. V Jayanti, K. M. McPeak, D. K. Kim, B. le Feber, F. Prins and D. J. Norris, *Nano Lett.*, 2019, **19**, 108.

48 A. Yang, T. B. Hoang, M. Dridi, C. Deeb, M. H. Mikkelsen, G. C. Schatz and T. W. Odom, *Nat. Commun.*, 2015, **6**, 6939.

49 E. T. Jaynes and F. W. Cummings, *Proc. IEEE*, 1963, **51**, 89.

50 M. Tavis and F. W. Cummings, *Phys. Rev.*, 1968, **170**, 379.

51 M. Tavis and F. W. Cummings, *Phys. Rev.*, 1969, **188**, 692.

52 J. A. Ćwik, S. Reja, P. B. Littlewood and J. Keeling, *EPL (Europhysics Lett.*, 2014, **105**, 47009.

53 D. Zhao, R. E. F. Silva, C. Climent, J. Feist, A. I. Fernández-Domínguez and F. J. García-Vidal, , DOI:2020, arXiv:cond-mat/2005.05657.

54 P. Michetti, L. Mazza and G. C. La Rocca, in *Organic Nanophotonics: Fundamentals and Applications*, ed. Y. S. Zhao, Springer Berlin Heidelberg, Berlin, Heidelberg, 2015, pp. 39–68.

55 E. Eizner, L. A. Martínez-Martínez, J. Yuen-Zhou and S. Kéna-Cohen, *Sci. Adv.*, 2019, **5**, eaax4482.

56 B. Liu, V. M. Menon and M. Y. Sfeir, *ACS Photonics*, 2020, **7**, 2292.

57 G. Groenhof, C. Climent, J. Feist, D. Morozov and J. J. Toppari, *J. Phys. Chem. Lett.*, 2019, **10**, 5476.

58 J. Galego, F. J. Garcia-Vidal and J. Feist, *Phys. Rev. X*, 2015, **5**, 041022.

59 J. Feist, J. Galego and F. J. Garcia-Vidal, *ACS Photonics*, 2018, **5**, 205.

60 J. Galego, F. J. Garcia-Vidal and J. Feist, *Nat. Commun.*, 2016, **7**, 13841.

61 J. Galego, F. J. Garcia-Vidal and J. Feist, *Phys. Rev. Lett.*, 2017, **119**, 136001.

62 H. L. Luk, J. Feist, J. J. Toppari and G. Groenhof, *J. Chem. Theory Comput.*, 2017, **13**, 4324.

63 O. Vendrell, *Chem. Phys.*, 2018, **509**, 55.

64 J. Fregoni, G. Granucci, M. Persico and S. Corni, *Chem*, 2020, **6**, 250.

65 J. Flick, M. Ruggenthaler, H. Appel and A. Rubio, *Proc. Natl. Acad. Sci.*, 2017, **114**, 3026.

66 J. Flick, H. Appel, M. Ruggenthaler, A. Rubio, H. Appel and A. Rubio, *J. Chem. Theory Comput.*, 2017, **13**, 1616.

67 J. Galego Pascual, *Polaritonic Chemistry*, Springer International Publishing, Cham, 2020.

68 J. A. Hutchison, T. Schwartz, C. Genet, E. Devaux and T. W. Ebbesen, *Angew. Chemie Int. Ed.*, 2012, **51**, 1592.

69 V. N. Peters, M. O. Faruk, J. Asane, R. Alexander, D. A. Peters, S. Prayakarao, S. Rout and M. A. Noginov, *Optica*, 2019, **6**, 318.

70 A. Thomas, J. George, A. Shalabney, M. Dryzhakov, S. J. Varma, J. Moran, T. Chervy, X. Zhong, E. Devaux, C. Genet, J. A. Hutchison and T. W. Ebbesen, *Angew. Chemie Int. Ed.*, 2016, **55**, 11462.

71 A. Thomas, L. Lethuillier-Karl, K. Nagarajan, R. M. A. Vergauwe, J. George, T. Chervy, A. Shalabney, E. Devaux, C. Genet, J. Moran and T. W. Ebbesen, *Science,* 2019, **363**, 615.

72 Y. Pang, A. Thomas, K. Nagarajan, R. M. A. Vergauwe, K. Joseph, B. Patrahau, K. Wang, C. Genet and T. W. Ebbesen, *Angew. Chemie Int. Ed.*, 2020, **59**, 10436.

73 K. Hirai, R. Takeda, J. A. Hutchison and H. Uji-i, *Angew. Chemie Int. Ed.*, 2020, **59**, 5332.

74 T. E. Li, A. Nitzan and J. E. Subotnik, *J. Chem. Phys.*, 2020, **152**, 234107.

75 J. A. Campos-Gonzalez-Angulo and J. Yuen-Zhou, *J. Chem. Phys.*, 2020, **152**, 161101.

76 V. P. Zhdanov, *Chem. Phys.*, 2020, **535**, 110767.

77 C. Climent, J. Galego, F. J. Garcia-Vidal and J. Feist, *Angew. Chemie Int. Ed.*, 2019, **58**, 8698.

78 B. Munkhbat, M. Wersäll, D. G. Baranov, T. J. Antosiewicz and T. Shegai, *Sci. Adv.*, 2018, **4**, eaas9552.

79 T. Virgili, D. Coles, A. M. Adawi, C. Clark, P. Michetti, S. K. Rajendran, D. Brida, D. Polli, G. Cerullo and D. G. Lidzey, *Phys. Rev. B*, 2011, **83**, 245309.

80 K. Stranius, M. Herzog and K. Börjesson, *Nat. Comm.*, 2018, **9**, 2273.

81 A. Thomas, A. Jayachandran, L. Lethuillier-Karl, R. M. A. Vergauwe, K. Nagarajan, E. Devaux, C. Genet, J. Moran and T. W. Ebbesen, *Nanophotonics*, 2020, **9**, 249.

82 I. M. Pastor and M. Yus, *Curr. Org. Chem.*, 2012, **16**, 1277.

83 R. M. A. Vergauwe, A. Thomas, K. Nagarajan, A. Shalabney, J. George, T. Chervy, M. Seidel, E. Devaux, V. Torbeev and T. W. Ebbesen, *Angew. Chemie Int. Ed.*, 2019, **58**, 15324.

84 D. B. Northrop, *Acc. Chem. Res.*, 2001, **34**, 790.

85 T. E. Li, J. E. Subotnik and A. Nitzan, *Proc. Natl. Acad. Sci.*, 2020, **117**, 18324.

86 H. Hiura, A. Shalabney and J. George, , DOI:10.26434/chemrxiv.7234721.v4.

87 H. A. Benesi and J. H. Hildebrand, *J. Am. Chem. Soc.*, 1949, **71**, 2703.

88 J. J. Pietron, K. P. Fears, J. C. Owrutsky and B. S. Simpkins, *ACS Photonics*, 2020, **7**, 165.

89 E. Laviron, *J. Electroanal. Chem. Interfacial Electrochem.*, 1984, **164**, 213.

90 J. A. Campos-Gonzalez-Angulo, R. F. Ribeiro and J. Yuen-Zhou, *Nat. Commun.*, 2019, **10**, 4685.

91 C. Rüssel and W. Jaenicke, *J. Electroanal. Chem. Interfacial Electrochem.*, 1984, **180**, 205.

92 N. T. Phuc, P. Q. Trung and A. Ishizaki, *Sci. Rep.*, 2020, **10**, 7318.

93 I. Vurgaftman, B. S. Simpkins, A. D. Dunkelberger and J. C. Owrutsky, *J. Phys. Chem. Lett.*, 2020, **11**, 3557.

94 S. Shin and H. Metiu, *J. Phys. Chem.*, 1996, **100**, 7867.

95 H. B. G. Casimir and D. Polder, *Phys. Rev.*, 1948, **73**, 360.

96 Casimir, H. B. G., *J. Chim. Phys.*, 1949, **46**, 407.

97 P. W. Milonni, *The Quantum Vacuum*, Academic Press, San Diego, 1994.

98 D. P. Craig and T. Thirunamachandran, *Molecular Quantum Electrodynamics: An Introduction to Radiation-Molecule Interactions*, Dover Publications, Inc., Mineola, New York, 1998.

99 A. Stone, *The Theory of Intermolecular Forces*, Oxford University Press, Oxford, 2nd edn., 2013.

100 C. Climent and J. Feist, *Phys. Chem. Chem. Phys.*, , DOI:10.1039/D0CP04154H.

101 C. Schäfer, M. Ruggenthaler, V. Rokaj and A. Rubio, *ACS Photonics*, 2020, **7**, 975.

102 J. Galego, C. Climent, F. J. Garcia-Vidal and J. Feist, , DOI:2018, arXiv:quant-ph/1807.10846v1.

103 J. Clayden, N. Greeves and S. Warren, *Organic Chemistry*, Oxford University Press, Oxford, 2nd edn., 2012.

104 A. N. Jay, K. A. Daniel and E. V. Patterson, *J. Chem. Theory Comput.*, 2007, **3**, 336.

105 R. Ramanan, D. Danovich, D. Mandal and S. Shaik, *J. Am. Chem. Soc.*, 2018, **140**, 4354.

106 P. Gamez, J. S. Costa, M. Quesada and G. Aromí, *Dalt. Trans.*, 2009, 7845.

107 H. J. Lin, D. Siretanu, D. A. Dickie, D. Subedi, J. J. Scepaniak, D. Mitcov, R. Clérac and J. M. Smith, *J. Am. Chem. Soc.*, 2014, **136**, 13326.

108 J. Cirera and E. Ruiz, *Inorg. Chem.*, 2016, **55**, 1657.

ABBREVIATIONS

BQ/dHQ: Benzoquinone/dihydroquinone

CBOA: Cavity Born-Oppenheimer approximation

EM: electromagnetic

EtOAc: ethyl acetate

HS: High-spin

LP: Lower polariton

LS: Low-spin

P3HT: 2,5-poly(3-hexylthiophene)

PES: Potential energy surface

PNP^{-}: para-nitro phenoxide

PNPA: para-nitrophenyl acetate

PoPES: Polaritonic potential energy surface

PTA: 1-phenyl-2-trimethylsilylacetylene

UP: Upper polariton

VSC: Vibrational strong coupling